Magnetic Targeted Drug Delivery

By

Jeffrey H. Leach

Thesis submitted to the Faculty of the
Virginia Polytechnic Institute and State University
in partial fulfillment of the requirements for the degree of

Master of Science
In
Electrical Engineering

Dr. Richard Claus, Chairman
Dr. Bradley Davis
Dr. Robert Hendricks

February 2003
Blacksburg, VA

Keywords: nanomagnetism, targeted drug delivery, magnetic microspheres,
magnetic stereotaxis system

Supported by Air Force Grant number #F49620-01-1-0407

Magnetic Targeted Drug Delivery

By

Jeffrey H. Leach

Abstract

Methods of guiding magnetic particles in a controlled fashion through the arterial system *in vivo* using external magnetic fields are explored. Included are discussions of applications, magnetic field properties needed to allow guiding based on particle characteristics, hemodynamic forces, the uniformity of field and gradients, variable tissue characteristics, and imaging techniques employed to view these particles while in transport. These factors influence the type of magnetic guidance system that is needed for an effective drug delivery system.

This thesis reviews past magnetic drug delivery work, variables, and concepts that needed to be understood for the development of an *in vivo* magnetic drug delivery system. The results of this thesis are the concise study and review of present methods for guided magnetic particles, aggregate theoretical work to allow proper hypotheses and extrapolations to be made, and experimental applications of these hypotheses to a working magnetic guidance system. The design and characterization of a magnetic guidance system was discussed and built. The restraint for this system that balanced multiple competing variables was primarily an active volume of 0.64 cm^3, a workspace clearance of at least an inch on every side, a field of 0.3T, and a local axial gradient of 13 T/m. 3D electromagnetic finite element analysis modeling was performed and compared with experimental results. Drug delivery vehicles, a series of magnetic seeds, were successfully characterized using a vibrating sample magnetometer. Next, the magnetic seed was investigated under various flow conditions *in vitro* to analyze the effectiveness of the drug delivery system. Finally, the drug delivery system was successfully demonstrated under limiting assumptions of a specific magnetic field and gradient, seed material, a low fluid flow, and a small volume.

Acknowledgments

I wish to acknowledge at Virginia Tech the support of my friends and co-workers at the Fiber and Electro-Optic Research Center, the Optical Sciences and Engineering Research Center, and Dr. Judy Riffle's group. The professors and researchers at this school have always made the time to answer questions and work through problems together. I am honored to have worked with such bold and intellectual people. I specifically wish to thank my advisor, Dr. Richard O. Claus, for his endless support in my research and life at Virginia Tech. I also would like to show my appreciation to Stereotaxis, Inc. and their staff, specifically Dr. Rogers Ritter and Dr. Duke Creighton. The Cleveland Clinic staff has also been very receptive and I would like to particularly thank Dr. Urs Hafeli for his support there. In addition I could have not done this without the continued love of God, friends, and family.

Table of Contents

List of Figures

List of Tables

Chapter 1: Overview

1.1 Introduction

The purpose of this thesis is to consider how externally applied magnetic fields can be used to guide materials internal to the body. The primary concern will be to examine current and prior attempts to discover a fusion of past designs that allow the guidance of magnetic microspheres. It is hypothesized that control of magnetic microspheres *in vivo* is feasible given a strong magnetic field and gradient space superpositioned on an arterial system. This work is fueled by the general nanotechnology initiative and the general desire for less invasive surgery using electromagnetic field-directed nanoparticles. The current nanotechnology initiatives are motivated by the added functionality derived from reducing the overall size of working systems. A general overview of the most important variables of concern and background is presented in the first section. Next, a review of prior and present magnetic field-based delivery systems will be explored. Modeling the controlling variables and their interactions are described in closer detail in the third section. Finally, in the fourth section, first-order experimental verification is performed to ensure the accuracy of the modeling. The end discussion summarizes results and provides recommendations for future research.

1.2 Background and Motivation

Magnetic microspheres have potential use as magnetic seeds for drug delivery. Such microspheres are paramagnetic and have been made to range in size from approximately one micron to greater then 600 microns. To control the motion of such microspheres within the body, a magnetic force due to an externally applied magnetic field and a hemodynamic drag force due to blood flow combine to create a total vector force on the spheres. In order to effectively overcome the influence of blood flow, and in order to achieve desired external magnetic field-controlled guidance, the magnetic force due to the external field must be larger than the drag force.

To a first approximation, the magnetic force on the microsphere is governed by

$$\vec{F} = \vec{\nabla}(\vec{m} \bullet \vec{B}_o), \quad \text{[Newtons]} \tag{1}$$

where **F** is the magnetic force, $\vec{m}$ is the total magnetic moment of the material in the microsphere, ∇ is the gradient, assumed in our modeling to be derived from characteristics of the **B** field alone, and **B** is the magnetic flux density, also known simply as the **B** field. Each of these quantities thus influences the degree to which an external magnetic field may be used to guide internal microspheres. The del operator, ∇, is defined as

$$\nabla \equiv \frac{\partial}{\partial x}\hat{a}_x + \frac{\partial}{\partial y}\hat{a}_y + \frac{\partial}{\partial z}\hat{a}_z \tag{2}$$[1]

in rectangular coordinates. It is noted that the gradient of a scalar function at any point is the maximum spatial change of the magnetic field at any point. The B field tends to align the net magnetic moment of the particle in a fixed direction while the gradient leads to a force that may move the particle. An extended analysis of magnetically-induced forces on magnetic materials is considered in Section 3.3 below. Figure 1 depicts an example magnetic field that would act on a magnetic particle.

Similar to rolling down a steep hill, the steeper the gradient is, the more total force will be placed on the particle. Table 1 gives typical B field values found in the universe and gives a sense of what values are realizable for a working magnetically controlled microsphere guidance system. Please refer to Appendix A for additional reference information of other magnetic variables and their corresponding units. The most challenging aspect of manipulating magnetic microspheres *in vivo* is the fact that the magnetic field and gradients weaken as $1/r^3$, so large fields are required for human patient-sized systems.

---

[1] Umran S. Inan, Aziz S. Inan. *Engineering Electromagnetics.* p. 277. Addison Wesley Longman, Inc. 1999.

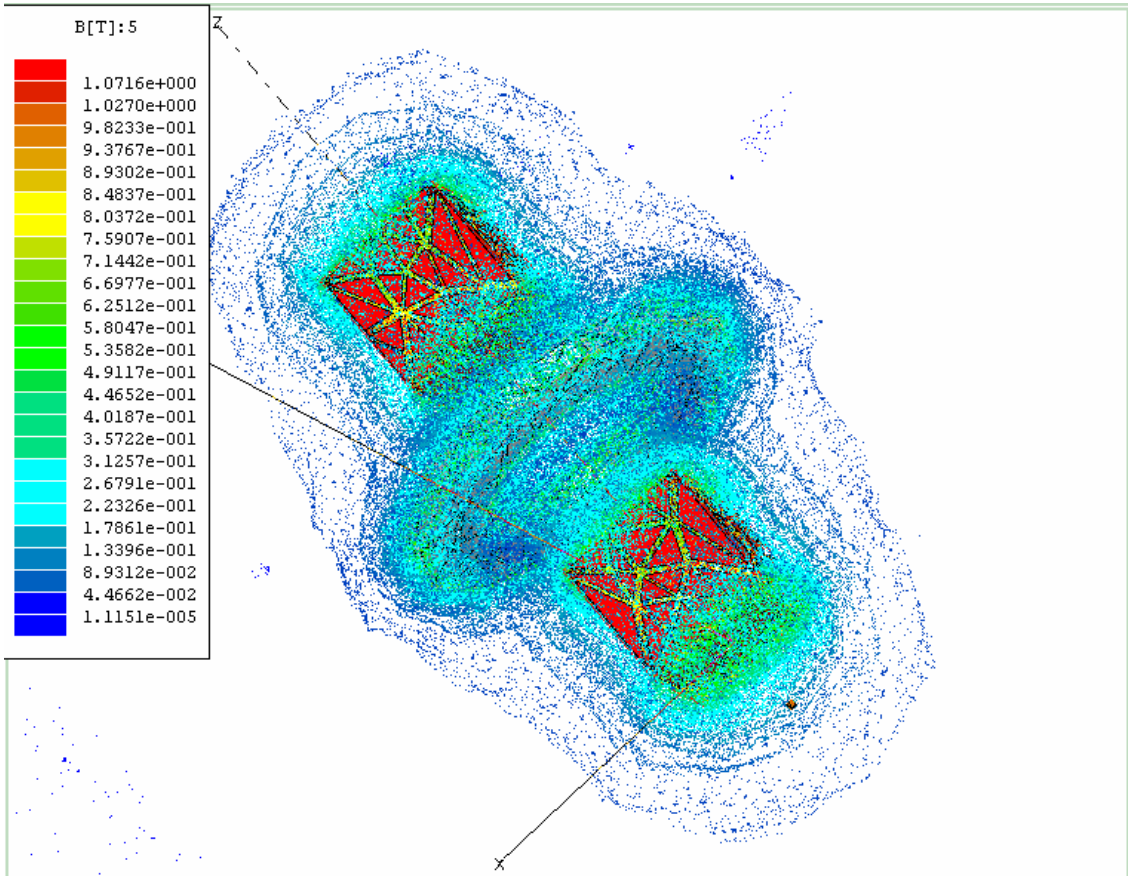

Figure 1. Example of a magnetic field distribution.

The second factor involves the magnetic properties of the microspheres. The magnetic moment of a material, **m**, is proportional to the applied field, H, and the intrinsic magnetic susceptibility of the material, χ_m.

$$\mathbf{m} = \chi_m H \qquad (3)$$

The magnetic volume susceptibility ranges for various materials from aluminum at 2.07 x 10^{-5} to magnetite at 1.0 x 10^6 -5.7 x 10^6 and as high as 10^6 for various ferromagnetic and rare-earth materials such as iron and gadolinium, respectively.[2,3] Thus by creating appropriately sized magnetic particles with sufficiently large $\bar{m}$, the resultant magnetic forces may be significant. It was expected that only a one order of magnitude increase in material susceptibility over magnetite may be attained using new and novel materials.

---

[2] Christopher P. Hunt, Bruce M. Moskowitz, Subir K. Banerjee. "Magnetic Properties of Rocks and Minerals". American Geophysical Union. p. 191, 1995.

[3] William D. Callister, Jr. *Materials Science and Engineering- an Introduction*. 5th ed: John Wiley & Sons, Inc., p. 681, 2000.

This small increase did not make changing materials a viable investment for the additional foreseen complications.

Table 1. Typical B field values in selected applications. [4,5]

Application	B field (Teslas)
Sensitivity of a scanning SQUID microscope	10^{-16}
Human Brain	10^{-13}
Intergalactic and interstellar magnetic fields	10^{-11}
Human heart	10^{-9}-10^{-8}
Earth's magnetic field	0.5×10^{-5}
Refrigerator magnets	10^{-4}- 8×10^{-3}
Electron beam of CRT	5×10^{-4}-10^{-3}
Magnetic read switch	10^{-3}- 2×10^{-3}
1-horsepower electric motor	0.1-0.2
Rare-earth permanent magnets	2
Magnetic Resonance Imaging	0.5-5
High-energy particle accelerators	10
World Record Continuous Field	45 T
Long-Pulse Magnet (800 ms)	60
Strongest Destructive Pulsed Magnet at NHMFL-Los Alamos (4-8 μs)	850
Neutron Stars	10^{8}

The force that counteracts the magnetic force on the particle in the bloodstream is due to blood flow. Stokes Law governs the hemodynamic forces on a particle in a flowing liquid.

$$\mathbf{F} = 6 \pi \eta v r, \qquad (4)$$

where **F** is the drag force, η is the viscosity of the fluid, v is the relative velocity of a spherical particle, and r is the radius.

---

[4] Umran S. Inan, Aziz S. Inan. *Engineering Electromagnetics.* p. 448. Addison Wesley Longman, Inc. 1999.

[5] Fritz Herlach. "Innovations and trends in magnet laboratories and techniques." Physica B. pp.294-295, 500-504.2001.

Other variables of concern internal to the body are tissue porosity to microspheres of certain size (and resulting $\vec{m}$), and allowable cell damage caused by incompatible microsphere sizes and forces. A highly porous tissue allows small microspheres to be easily manipulated out of the bloodstream and into the tissue. However, a relatively tight tissue structure would require more magnetic field-induced force to pull the microspheres out of the bloodstream and such interfacial transport could cause damage to the tissue. Therefore, the microsphere size and forces needed for effective microsphere manipulation are highly dependent on the area in which drug delivery is to be performed.

The motivation for this project comes from the numerous potential applications for a magnetic field-controlled drug delivery system. Targeted microsphere delivery platforms have the ability to deliver simultaneous medical applications of gene therapy[6], destroy built up plaque in arteries, image and extract foreign metallic and ferric objects from the body, and affect cancer therapies of in-vitro vesicular blockage[7], targeted radiation therapy[8], and hyperthermia[9].

Drug targeting would allow a lower whole body dosage of medicines and treatments that otherwise would not be a viable solution to a problem due to the toxicity of higher doses. An example of this is Dr. Kurt Hofer's work with hyperthermia[10]. Hofer was able to make cancerous cells more susceptible to heat compared to normal cells by introducing

---

[6]C. Plank, F. Scherer, U. Schillinger, M. Anton, C. Bergemann. "Magnetofection: Enhancing and Targeting Gene Delivery by Magnetic Force." Fourth International Conference on the Scientific and Clinical Applications of Magnetic Carriers. 67-70, 2002.

[7] G.A. Flores and J. Liu. "In-vitro blockage of a simulated vascular system using magnetorheological fluids as a cancer therapy." Fourth International Conference on the Scientific and Clinical Applications of Magnetic Carriers. 19-21, 2002.

[8] Hafeli, U., Pauer, G., Failing, S., Tapolsky, G. "Radiolabeling of Magnetic Particles with Rhenium188 for Cancer Therapy", Journal of Magnetism and Magnetic Materials. Vol. 225 p.73-78, 2001.

[9] Kurt Hofer. "Hyperthermia and Cancer." Fourth International Conference on the Scientific and Clinical Applications of Magnetic Carriers. 78-80, 2002.

[10] Kurt Hofer. "Hyperthermia and Cancer." Fourth International Conference on the Scientific and Clinical Applications of Magnetic Carriers. 78-80, 2002.

misonidazole, which takes advantage of the observation that cancerous cells use more oxygen than normal cells. The cancerous cells absorbed misonidazole more than normal cells, thus making the cancerous cells more susceptible to heat. When heat was applied to the area, the cancer cells died faster then the surrounding normal cells. This was a faster method of curing cancer compared to the routine multifraction radiotherapy. The major problem with this treatment is that buildup in the brain of this drug causes neuropathy 10-12 months later. Careful delivery and removal of toxins for such local site activation could be accomplished with magnetic drug delivery.

Analysis of development of magnetically targeted drug delivery systems.

The first step in the design of such a system is to choose a seed material. For experimental work discussed below ferromagnetic magnetite (Fe_3O_4) was chosen due to its relatively high magnetic moment in reasonably sized particles and because of the amount of work that has be done to demonstrate its relatively low toxicity in the body when encapsulated in a protective protein cage. [11]

The next design step is to incorporate this magnetic seed with different drugs. Encapsulation of the drugs with magnetite shells or attaching the drugs to a functionalized outer coating may be performed. Functionalized outer coatings of microspheres are a well-established procedure.[12] Such modified magnetic microspheres may then be delivered to the target cells, where the microspheres will decompose due to their poly-lactic acid or other degradable coating, and the drug will be delivered.

---

[11] Linda A. Harris. "Polymer Stabilized Magnetite Nanoparticles and Poly(propylene oxide) Modified Styrene-Dimethacrylate Networks." Dissertation Submitted to Virginia Polytechnic Institute and State University, April 19, 2002.

[12] Tech Notes. Bang Labs, Inc. http://www.bangslabs.com/support/index.php

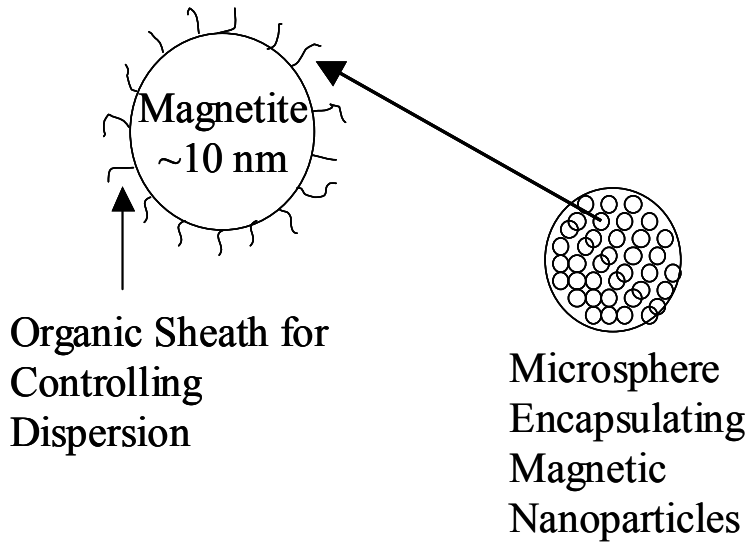

Figure 2. Preservation of single domains.

Each of the microspheres contains multiple magnetite molecules. A magnetic domain is a volume of material whose magnetic field is aligned in a given direction. When magnetite is smaller than approximately 30 nm in diameter only single magnetic domains form. Magnetite clusters larger than 30 nm start to interact and form a multiple domain material. In single domain materials there is little to no hysteresis and the magnetic particles reach saturation faster compared to a multi domain material. The data from a vibrating sample magnetometer (VSM) confirm that only single domains formed in the small microspheres that we studied. If multiple domains were formed we would notice a hysteresis loop in the magnetization curves. This hysteresis from multi domain formation would cause a decrease in the response of the system. The organic sheaths surrounding the magnetite clusters provide both the ability to functionally attach drugs as well as to keep the magnetic particles from aggregating, preserving single domain formation (Figure 2). Finally, the design of a magnetic guidance system is developed with the previous constraints in mind.

Chapter 2: Past Design Strategies

2.1 Introduction

There have been many attempts in the past to create platform technologies that can guide and deliver drugs, make repairs, and essentially give one's hands the dexterity to seamlessly manipulate nature from macro and micro sizes to the nanometer scale. This range of maneuverability and control over matter allows noninvasive surgery and the ability to pass through tissue and even cell walls instead of cutting or lysing them to obtain internal access to a material or body. D. Montgomery et al. conceived the first multicoil superconducting magnetic manipulator in 1969[13]. Commercially it appears that only Stereotaxis, Inc. and FeRx Inc. are working on FDA approval for various magnetic targeted drug delivery methods.

One large commercial area of magnetic manipulation that has been completed is in the use of magnets to manipulate and retrieve foreign ferric objects in the eye. Examining Table 2 we take note of the various magnet designs and their applications. Some of these applications also include retinal tear repair and cataract emulsification.

Another extensive area that has been investigated is the use of magnetic manipulation to perform noninvasive surgery on the cardiologic and endovascular systems. These systems represent a significant percentage of the human body and further demonstrate the wide range of applications that can be performed with magnetic targeting. The experiments documented in Table 3 demonstrate angiography, stripping varicose veins, removing plaque deposits, chemotherapy and aneurysm embolization.

---

[13] D Montgomery, R.J. Weggel, M.J. Leupol, S.B. Yodh, and R.K. Wright. J.Appl. Phys. 40, 2129 (1969).

Table 2. Design and performance characteristics of selected ophthalmic magnetic manipulation systems used since the 1950s.[14]

Authors	Apparatus/ Method	Application	Design Features	Results	Year
M.F.McCaslin[15]	Pulsed-field, high-gradient electro-magnet	Removal of intraocular foreign bodies (non-specific injuries)	50% Fe – 50% Co core, 34 cm long x 7.4 cm diam., 120° pole-place tip angle	Maximum gradient = 650 T/m within 1 cm of probe tip	1958
N.R. Bronson II[16]	Storz-Atlas (S-A) magnet, Bronson-Magnion pulsed magned	Comparison of pulling force vs. tip geometry and temperature	Solid-state Hall-effect transducers used to map the tip's field gradient	B-H magnet has pulling force = 7x that of S*A magnet (@50% duty cycle)	1968
R.J. AmaLong[17]	Lancaster-Geiger magnet, Bronson-Magnion magnet	Removal of intraocular foreign bodies (shrapnel injuries)	Hand-held magnets used in conjunction with cryothermic wound closure	Foreign objects > 3mm may detach retine unless approached posterioly	1970
G. Landwehr et al. [18]	Pulsed-field, hand-held magnet, and axial inner-pole magnet	Improved-control method for extracting intraocular foreign bodies	10-ms pulse sequence used a 50% duty cycle, test particle mass = 0.043g	Oscillatory relaxtion time – 100ms, object moved in steps of = 0.4 mm./sequence	1977
G.M. Stephens et al. [19]	Standard ophthalmic hand manget, curved and straight tips	Measurement of the distribution of magnetic flux surrounding tip	Magnet operated at 120 V over a current range of 100 – 400mA	1 mg object must be < 8mm from magnet tip to move in vitreous @ 400 mA	1977
D. Lobel et al[20]	Magnetically guided intraocular sphere, (Teflon coated)	Unfolding of overlapped retina followed, by repair of retinal tear	Sphere diam. Range-0.5 to 6.0 mm; magnet-tipped diathermy probe guides sphere	In vivo studies showed no retinal bleeding, but some flattening and	1978

[14] G.T. Gillies, R.C. Ritter, W.C. Broaddus, M.S. Grady, M.A. Howard III, R.G. McNeil. "Magnetic Manipulation Instrumentation for Medical Physics Research" Rev. Sci.Instrum. 65 (3), March 1994.
[15] M F. McCaslin, Trans. Am. Ophthalmol. Sot. **56**, 571 (1958).
[16] N. R. Bronson II, Arch. Ophthal. **79**, 22 (1968).
[17] R. J. Amalong, Am. J. Ophthal. **70**, 10 (1970).
[18] G. Landwehr, K. Dietrich, H. Weber, W. Bushmann, and H. Neubauer,Ophthalmic Res. 9, **308** (1977).
[19] G. M. Stephens, A. A. Cinotti, A. R. Caputo, E. P. Veltri, and A. A. Vigorito, in Proceedings of the San Diego Biomedical Symposium, edited by J. I. Martin (Academic, New York, 1977), Vol. 16, pp. 387-390.

Authors	Apparatus/ Method	Application	Design Features	Results	Year
				compression	
D. J. Coleman[21]	Bronson-Magnion pulsed magnet with customized tips	Comparison of pulling force vs. tip geometry	Tip extension improves the access to foreign body and minimizes extraction damage	Coleman "straight" tip and Bronson "long" tip produce B= 2,000 G at 2 cm from tip.	1982
A. Schumann, Inc. [22]	High-field giant magnet with conical coil and iron core	Explosion-proof system for removal on intraocular foreign bodies	Five-step power regulating switch thermostatic shutoff to prevent overheating	Field strength of 1.3 T at tip, 0.5 T at 1 cm, and 0.3 T at 2 cm	1982
H. Weber et al[23,24]	Magnetically driven introcular oscillator (two external coils)	Determination of the compliance and damping of the vitreous	Spheres of 0.5 to 1.0 mm diam. Driven at 1 to 60 Hz by two pulsed coils	7.6×10^4 $H*m^{-3}$ = spring constant per unit area of in vitro human vitreous	1982
D.R. May et al. [25]	Modified 20-gauge tip for Bronson intraocular electromagnet	Extraction of foreign bodies by insertion of tip through pers plana	Standard Bronson acorn tip machine down to cyline 20-gauge diam. X 5 mm long	Apparatus has been used successfully in ~ 10 human-clinical trials	1989
Aura Systems, Inc. [26]	Computer-aided, multi-coil magnetic manipulation ("KELMAST")	Cataract emulsification via high-speed rotation of an implanted object	Currents in four conical coils controlled by surgeon via joystick	"magnabit" inserted through 1-mm incision; feedback cancels vibrational effects	1992

[20] D. Lobel, J. R. Hale, and D. B. Montgomery, Am. J. Ophthalmol. **85**,699 (1978).
[21] D. J. Coleman, Am. J. Ophthalmol. **85**, 256 (1978).
[22] Schumann GM3F & GM3FEX Giant Eye Magnets" (A. Schumann,Inc., West Concord, Massachusetts, August, 1982), 4 pp.
[23] H. Weber and G. Landwehr, Ophthalmic Res. 14, 326 (1982).
[24] H Weber, G. Landwehr, H. Kilp, and H. Neubauer, Ophthalmic Res. 14, 335 (1982).
[25] D. R. May, F. G. Noll, and R. Munoz, Arch. Ophthalmol. 107, 281(1989).
[26] S. Burke, B. Laufer, E. Leibzon, A. Schwartz, M. Strugach, R. Van Allen, and C. Warren, Magnetically Assisted Cataract Surgery: Overview (Aura Systems, Inc., El Segundo, California, October 27, 1992), 2 pp.

Table 3. Design and performance characteristics of selected cardio/endovascular magnetic manipulation systems used since the 1950s. [27]

Authors	Apparatus/ Method	Application	Design Features	Results	Year
H. Tillander[28,29,30]	Permanent-magnet-tipped catheter guided by electromagnet	Selective angiography of canine pancreaticoduodentre nal artery	Multi-magnet catheter tip, made of Platinax-II cylinders, max. diam. = 2.1 mm	x-ray image intensifier required screening with 2 layers of 2-mm Mumetal	1951
H.T. Modny et al. [31]	Transvenous plumb-line navigated through the vein by external magnet	Minimally invasive technique used for stripping varicose veins	Magnetically attracted probe mass draws stripping cord through the vein.	Only two incisions needed to facilitate entrance, exit and guidance of cord	1958
E.H. Frei et al. [32,33,34]	Para-operational device ("POD"), vix., magnet-tipped catheter	Placement of intravascular transducers, drug delivery and biopsy	Permanent magnet tip ~ 1 mm diam. X 5 mm long with soft rubber sheath as cover	Several different versions of device built and used in human clinical trials	1963
S.B. Yodh et al. [35]	Catheter guidance via two goniometer-mounted 2.5 kW electromagnets	Delivery of contrast agents, chemotherapy, aneurysm embolization	Pt-Co magnet-tips, 1.3 mm diam., with heat-soluble paraffin link to catheter	> 90° turn-angle achieved during in vivo study in rabbit renal-vein system	1968
J. A. Taren and T.O. Gabrielsen[36,37]	Transvascular magnetic electrode catheter, ac-dc guide magnet	RF-lesioning of extra-cranial arteriovenous malformations (humans)	Sm-Co magnet, .5 mm diam. X 1.5 mm long on coiled electrode inside catheter	Guidance range ~ 12 cm, 3-mm thrombi produced via RF heating of catheter tip	1970

[27] G.T. Gillies, R.C. Ritter, W.C. Broaddus, M.S. Grady, M.A. Howard III, R.G. McNeil. "Magnetic Manipulation Instrumentation for Medical Physics Research" Rev. Sci.Instrum. 65 (3), March 1994.
[28] H. Tillander, Acta Radiol. 35, 62 (1951).
[29] H. Tillander, Acta Radiol. 45, 21 (1956).
[30] H. Tillander, IEEE Trans. Magn. MAC-4 355 (1970).
[31] M. T. Modny, G. Ridge, and J. P. Bambara, U.S. Patent No. 2 863 458 (9 December 1958).
[32] E. H. Frei, S. H. Leibinsohn, H. N. Heufeld, and H. N. Askenasy, in Proceedings.of the 16th Annual Conference on Engineering in Medicine and Biology, edited by D. A. Robinson (Harry S. Scott, Inc., Baltimore, MD, 1963), Vol. 5, pp. 156-157.
[33] E. H. Frei, J. Driller, H. N. Neufeld, I. Barr, L. Bleiden, and H. M. Askenasy, Med. Res. Eng. 5, 11 (1966).
[34] ME. H. Frei and S. Leibmsohn, U.S. Patent No. 3 358 676 (19 December 1967).

[35] B. Yodh, N. T. Pierce, R. J. Weggel, and D. B. Montgomery, Med. Biol. Eng. 6, 143 (1968).
[36] J. A. Taren and T. 0. Gabrielsen, Science 168, 138 (1970).

Authors	Apparatus/ Method	Application	Design Features	Results	Year
J.H. Sobiepanek[38]	Magnetically-guided catheter with cibrating plunger in tip	Percussive destruction of blockages in the coronary arteries	Externally-applied, pulsed magnetic field causes the plunger to reciprocate	Design studies showed that probes 2.3 mm diam x 15 mm long were feasible	1970
D.B. Montgomery et al. [39]	Catheter guidance via one goniometer-mounted 2.5 kw electromagnet	Catherization of internal carotid artery and its divisions	0.5 mm Silastic™ catheter with 0.9 mm diam. Pt-Co tip monitored by fluroscope	Catheter has reached the anterior communicating junction oin four human trials	1970
D.H. Ledermen et al. [40]	Intravascular magnetic suspension of test objects in pulsatile flow	In vivo assessment of hemocompatbiliity of prosthetic materials	Test device ~ 5 mm diam x 50 mm long; Hall probes sense test device position	Feasibility of non-contact suspension demonstrated in canine aorta (in vivo)	1977
W. Ram and H. Meyer[41]	Permanent-magnet tipped polyurethane angiography catheter	Intraventricular catheteriation in heart of neonate	1.2 mm diam x 8 mm long magnetic tip in 4.7F catheter; x-ray visualization	Catheter steerable up to 40 mm from external magnet, no complications during use	1991

Further, gastro-intestinal track magnetic manipulation, such as the prior work indicated in Table 4, demonstrates the feasibility of guidance under different flow conditions and size restrictions. Demonstrated applications include resolving intestinal obstructions, tissue biopsies, increased visualization with magnetic contrasts, and repositioning of tissue for radiation treatment.

---

[37] J. A. Taren and T. 0. Gabrielsen, IEEE Trans. Magn. MAC-C, 358 (1970).
[38] J. M. Sobiepanek, IEEE Trans. Magn. MAC-6, 361 (1970).
[39] D. B. Montgomery, J. R. Hale, N. T. Pierce, and S. B. Yodh, IEEE Trans. Magn. MAGQ 374 (1970).
[40] D. M. Lederman, R. D. Gumming, H. E. Petschek, T.-H. Chiu, E. Nyilas, and E. W. Salzman, AM Acad. Sci. (N.Y.) 283, 524 (1977).
[41] W. Ram and H. Meyer, Cathet. Cardiovas. Diag. 22, 3 17 (1991).

Table 4. Design and performance characteristics of selected gastroenterology magnetic manipulation systems used since the 1950s. magnetic manipulation systems used since the 1950s. [42]

Authors	Apparatus/ Method	Application	Design Features	Results	Year
J.W. Devine and J.W. Deine, Jr. [43]	Magnetic guidance of flexible tube with high permeability tip	Duodenal intubation for emergency surgery or intensinal obstruction	Fluoroscopic visualization of probe manipulation via external Alinico 5 magnet	Human clinical trials established tube controllability in stomach	1953
H.F. McCarthy et al. [44,45,46]	Magnetic guidance of flexible tube with permanent magnet tip	Gastral intubation through the pylorus into the duodenum	Alinico-5 tip in Cantor, MillerAbbot or Levin tube steered by external dc coil	Human clinical trials demonstrated guidance range of 20 cm	1961
F.E. Luborsky et al. [47]	Steerable spring-loaded magnetic probe for control of field strength	Magnetotractive endoscopy for retrieval of foreign objects	Shielded 6-mm diam. Alinico-5 magnet contacts soft iron pole tip to attract target	"on-off" control of field enables selective actuation; stray flux < 4% when "off"	1964
J. Driller and G. Neumann[48]	Electronically drive, magnetically activated biopsy device	Acquisition and removal of 2-mm diameter tissue samples from GI tract	Alinico magnet with attached cutting ring is plunger for remotely close relay	Vacuum aspiration controls sample size; SCR closure pulse duration ~ 15 ms.	1967
E.H. Frei et al. [49,50]	Magnetic manipulation of ferromagnetic contrast agents	x-ray screening and visualization of the stomach and intestines	Solid solution of magnesium ferrites and oxides manipulated by Alinico-5 magnet	Human trials demonstrated useful control and imaging of stomach and intenstine	1968

[42] G.T. Gillies, R.C. Ritter, W.C. Broaddus, M.S. Grady, M.A. Howard III, R.G. McNeil. "Magnetic Manipulation Instrumentation for Medical Physics Research" Rev. Sci.Instrum. 65 (3), March 1994.
[43] J. W. Devine and J. W. De&e, Jr., Surgery 33, 513 (1953).
[44]H. F. McCarthy, H. P. Hovnanian, T. A. Bremran, P. Brand, and T. J. Cummings, in Digest of the I961 International Conference on Medical Electronics, edited by P. L. Frommer (McGregor & Werner, Washington, DC, 1961), p. 134.
[45]H. F. McCarthy, H. P. Hovnanian, T. A. Brennan, and P. L. Gagner, Surgery 50, 740 (1961).
[46]H. F. McCarthy, U.S. Patent No. 3 043 309 (10 July 1962).
[47]F. E. Luborsky, B. J. Drummond, and A. Q. Penta, Am. J. Roentgenol. 92, 1021 (1964).
[48]J. Driller and G. Neumann, IEEE Trans. Biomed. Eng. BME-14, 52.(1967).
[49]E. H. Frei, E. Gunders, M. Pajewsky, W. J. Alkan, and J. Eshchar, J. Appl. Phys. 39, 999 (1968).

Authors	Apparatus/ Method	Application	Design Features	Results	Year
F.C. Izsak et al.[51]	Magnetic manipulation of iron pellets in the bowel by external field	Reposition of small bowel during radiation treatment of cancer	Pellet location in bowel monitored by x-rays for 12-hour period	Human trial demonstrated ability of external field to manipulate bowel loops	1974
E. Frei and S. Yerushaimi[52]	Magnetic manipulation of GI catheter that contains iron beads	Repositioning of small bowel during radiation treatment of cancer	Catheter length was ~ 1m; outer diameter ~ 3 to 7 mm; field strength ~ 6 kOe	Human trial demonstrated ability of external field to manipulate bowel loops	1975
W. H. Hendren and J.R. Hale[53,54]	Magnetic attraction of tethered gastroimplants via air-core solenoid	Treatment of esophageal atresia by stretching the separated tissues	20-kW dc electromanget attracts two 9-mm diam. X 20-mm long gastroimplants	Throat and tissue pouches stretched until they meet, then surgically joined	1975
R.B. Jaffe and H.H Corneli[55]	Magnet-tipped orogastric tube and Foley catheter	Retrieval of foreign objects ingested by children	Silastic™ orogastric tube ~ 4 mm diam.; magnetic tip ~ 5 mm diam. X 25 mm long	Tube/magnet passed into the stomach; x-ray views aid engagement of target object	1984
E. Volle et al.[56,57]	FE-EX® OGTM catheter with cylindrical permanent magnet	Intubation of the esophagus for retrieval of foreign objects	Sm-Co Vacomax® 200 magnet and 50-cm catheter used in the original studies	Commercial-grade apparatus used in thirteen cases; length of procedure < 3 min	1989

[50] M. Pajewsky, J. Eshchar, W. J. Alkan, S. Yerushalmi, and E. H. Frei, IEEE Trans. Magn. MAG-6, 350 (1970). IEEE Trans. Magn. MAG-6, 350 (1970).
[51] F. C. I&k, H. J. Brenner, J. Tugendreich, S. Yerushalmi, and E. H. Frei, IEEE Trans. Magn. MAG-6, 350 (1970).
[52] E. H. Frei and S. Yerushalmi, U.S. Patent No. 3 794 041 (26 February 1974).
[53] J. R. Hale, IEEE Trans. Magn. MAG-11, 1405 (1975).
[54] W. H. Hendren and J. R. Hale, N. Engl. J. Med. 293, 428 (1975).
[55] R. B. Jaffe and H. M. Comeli, Radiology 150, 585 (1984).
[56] E. Voile, D. Hanel, P. Beyer, and H. J. Kaufmann, Radiology 160, 407.(1986).
[57] E Volle, P. Beyer, and H. J. Kaufmann, Pediatr. Radiology 19, 114(1989).

Authors	Apparatus/ Method	Application	Design Features	Results	Year
R.B. Towbin et al. [58]	High durability, distally curved Medi-tech magnetic catheter	Intubation of the esophagus for retrieval of oreign objects	Nylon-reinforced poly ethylene catheter with stainless steel housing for magnet	Magnetic hold force > 30 g; Foley catheter not needed to pass cricopharyngeus muscle	1990

Table 5 gives a detailed comparison of prior magnetic system designs that do not employ stereotactic manipulation (the manipulation of an object to an externally fixed reference frame). These methods have advantages in that they can quickly retrieve and use magnetic objects without expensive bio-imaging techniques, however they have limited areas of use in the body that do not require open surgery. One noteworthy point is the manipulation by S.K. Hilal in 1969 using a gradient of 0.275 T/m. The delivery of a ferrofluid consisting of multiple magnetic microspheres is of direct concern with these designs. Also, of worthy note is the successful suspension and aneurysm occlusion by D.A. Roth in 1969.

The pulmonary system has its own unique challenges and obstacles. Typically the chest is one of the largest cavities in the body and therefore it represents one of the most difficult areas for an external magnetic field and gradient to manipulate a ferric object due to the distance/field tradeoff indicated above. Of additional importance is that lung cancer is the leading cause of death from all cancer sites[59], so magnetic-directed therapies are attractive alternatives to conventional methods. Highlighted applications demonstrated include biopsy, stretching of tissues, and the manipulation of a probe for better lung monitoring.

[58] R. B. Towbin, J. S. Dunbar, and S. Rice, AJR 154, 149 (1990).
[59] Cancer Facts & Figures 2002. American Cancer Society. http://www.cancer.org

Table 5. Design and performance characteristics of selected nonstereotactic neurosurgical magnetic manipulation system used since the 1960s to guide catheters or concentrate ferromagnetic slurries. [60]

Authors	Apparatus/ Method	Application	Design Features	Results	Year
J.F. Alkane et al. [61]	Magnetically controlled intracranial thrombosis with iron powders	Obliteration of intracranial aneurysms (to prevent rupture)	Alinico V permanent magnet implanted in contact with aneurysm to create thrombus	Three human clinical trials carried out with burr-hole entrance for implanted magnet.	1966
J.F. Alksne[62]	Magnetically controlled intravasculat catheter	Obliteration of intracranial aneurysms and selective angiography	C-shaped electromagnet with 10-cm gap used to guide iron-tipped catheter tube	30 A in coil needed for 10^3 cc/minute flow; in vivo canine trials successful	1968
D.A. Roth[63]	Magnetically controlled intracranial thrombosis with iron microspheres	Obliteration of intracranial aneurysms (to prevent rupture)	Two conically tipped, 3-mm diameter Alnico V magnet attract the iron particles	50 cc suspension of microspheres injected in human trial; aneurysm occluded	1969
S.K. Hilal et al. [64,65,66]	POD catheter guided by external magnetic fields	Exploration of small vessels and aneurysm obliteration	Catheter with Alinico tip, 0.7 x 3.0 mm, guided by field gradient of 27. 5 G/cm	Selective catherization of middle cerebral artery in man via arotid-artery entry	1969
J.Holcho et al. [67,68]	POD catheter guided by external magnetic fields	Delivery of crytoxic materials to brain tumors	SCR-inverter-based square wave power supply used to coil power manipulation coil	Methotrexate sodium placed in tumors via middle cerebral artery in 3 human trials	1970

[60] G.T. Gillies, R.C. Ritter, W.C. Broaddus, M.S. Grady, M.A. Howard III, R.G. McNeil. "Magnetic Manipulation Instrumentation for Medical Physics Research" Rev. Sci.Instrum. 65 (3), March 1994.
[61] J. F. Alksne, A. G. Fingerhut, and R. W. Rand, Surgery 60, 212.(1966).
[62] J. F. Alksne, Surgery 64, 339 (1968).
[63] D. A. Roth, J. Appl. Phys. 40, 1044 (1969).
[64]S. K. Hilal, W. J. Michelsen, and J. Driller, J. Appl. Phys. 40, 1046. (1969).
[65]J. Driller, S. K. Hilal, W. J. Michelsen, B. Sollish, L. Katz, and W. Konig, Jr., Med. Res. Eng. 8, 11 (1969).
[66]OS. K. Hilal, J. Driller, and W. J. Michelsen, Invest. Radiol. 4, 406. (1969).
[67]Molcho, H. Z. Kamy, E. H. Frei, and H. M. Askenasy, IEEE Trans. Biomed. Eng. BME-17, 134 (1970).

Authors	Apparatus/ Method	Application	Design Features	Results	Year
J. Driller et al. [69]	POD-like catheter guided by external magnetic fields	Embolization of AVMs by silastic-coated magnet that "pops-off"	DOW 602-105 tubing used as distel catheter tip coated with DOW Type A Silasticia	Human trials carried out of AVM fed by lenticulostriate arteries	1972
H. L. Cares et al. [70]	Magnetically guided "macroballoon" released by RF induction heating	Obliteration of intrcranial aneurysms and selective angiography	380-kHz RF field used to heat catheter tip, thus sealing latex balloon	Technique used on aneurysms created in canines, balloons filled via 25% serum albumin	1973
T. Kusunoki et al. [71]	Magnetically controlled catheter with "intra-cranial balloon"	Obliteration of intracranial aneurysms via guided balloon	Room-temperature coil used; 300 turns of 0.8 mm wire on 42-mm dimater iron rod	Guidance achieved in pulsed water flow and in canine trial of vein pouch aneurysm	1982
A. Gaston et al. [72]	Catheter guidance via superconducting coil on articulated arm	Treatment of arteriovenous fistulae and vascular aneurysms	0.2 mm diam x 1.5 mm long Sm-Co magnetic tip. coil gradient ~ 10 T/m @ 10 cm	Catheter -guided balloons used to occlude aneurysms in canine in vivo studies	1988

The investigation of exploratory magnetic manipulation systems is important since they can be used in conjunction with an untethered magnetic drug delivery system to further localize usage of a drug. Of most noteworthy concern is the detailed engineering and design study D. Montgomery et. al performed. This study was the basis for the fifth generation magnetic stereotaxis system (MSS) that was developed in cooperation with Stereotaxis, Inc.

---

[68] H. M. Askenasy, H. Z. Kamy, E. H. Frei, and J. Molcho, IEEE Trans. Vol. 6, p. 89. Magn. MAG-6, 375 (1970).
[69] J. Driller, S. K. Hilal, W. J. Michelsen, and R. D. Penn, in Proceedings of the 25th Annual Conference on Engineering in Medicine and Biology, edited by S. P. Asper (McGregor $ Werner, Washington, D.C., 1972), Vol. 14, p. 306.
[70] L. Cares, J. R. Hale, D. B. Montgomery, H. A. Richter, and W. H. Sweet, J. Neurosurg. 38, 145 (1973).
[71] 14T. Kusunoki, S. Noda, N. Tamaki, S. Matsumoto, H. Nakatani, Y. Tada, and H. Segudhi, Neuroradiol. 24, 127 (1982).
[72] A. Gaston, C. Marsault, A. Lacaze, P. Gianese, J. P. Nguyen, Y. Keravel, A. L. Benabid, P. Aussage, and J. P. Benoit, J. Neuroradiol. 15, 137 (1988).

Table 6. Design and performance characteristics of selected magnetic manipulation systems used in orthopedic, urological, and pulmonary applications since the 1960s.[73]

Authors	Apparatus/ Method	Application	Design Features	Results	Year
D. Grob and P. Steign[74]	Electromagnetic field acting on probe masses fixed to internal organ	Restoration of bladder function via controlled compression	8-kw electromagnet used to generate a field of 0.17 T and gradient of 11.0 T/m	Canine trials demonstrated magnetically driven voiding rate of 1.3 cc/s	1969
W.J. Casarella et al. [75]	Modified POD-style bronchial catheter	Selective catherization of pulmonary bronchial segments	Polyethylene tubing with silicone-rubber distal eng and Alnico V magnetic tip	Selective bronchography carried out in two human clinical trials	1969
J. Driller et al. [76,77]	Modified POD –style bronchial catheter	Guidance of bronchial biopsy devices and medication delivery	Gas-sterilized POD assembly with Alnico V magnetic tip and pressure relief valve	Dental-broach-tipped biopsy wire used in human trials to obtain lesion tissue	1970
D. Grob and P. Stein[78]	Externally mounted magnetically palpebral eyelid prosthesis	Correction of ptosis due to muscle disease of congenital causes	1 x 2 x 2-mm Sm-Co magnets embedded in a polyurethane arc; mass of assembly ~ 1g	Magnetic arc on upper eyelid attracts ferrous strip on lower; tested on patients	1971
D. Grob and P. Stein[79,80]	Magnetically controlled U-shaped spring-clamp prosthesis	Management of urinary incontinence and bladder dysfunctions	Clamp is 3 cm long, 1.5 cm wide, with 2.2g soft steel closure mass on one leaf	Field of 0.05 T and gradient of 2.5 T/m opened clamp for micturition in canine trials	1971

[73] G.T. Gillies, R.C. Ritter, W.C. Broaddus, M.S. Grady, M.A. Howard III, R.G. McNeil. "Magnetic Manipulation Instrumentation for Medical Physics Research" Rev. Sci.Instrum. 65 (3), March 1994.
[74] D. Grob and P. Stein, J. Anal. Phvs. 40. 1042 (1969).
[75]W. J. Casarella, J. Driller, &d S. K. Hilal, Radiblogy'93, 930 (1969).
[76] J Driller, W. J. Casarella, T.Asch, and S. K. Hilal, IEEE Trans. Magn. MAGQ, 353 (1970).
[77] J. Driller, W. J. Casarella, T. Asch, and S. K. Hilal, Med. Biol. Eng. 8, 15 (1970).
[78] D. Grob and P. Stein, J. Appl. Phys. 42, 1318 (1971).
[79] D. Grob and P. Stein, J. Appl.. Phys. 42, 1331 (1971).
[80] D. Grob and P. Stein, IEEE Trans. Magn. MAG-8, 413 (1972).

Authors	Apparatus/ Method	Application	Design Features	Results	Year
D.J. Cullen et al. [81]	Differential mutual inductance sensor monitors susceptible mass	Controlled placement of endotracheal tubes in anesthetized patients	3-mm wide, 25 μm thick Mu-Metal band fused on tube; location displayed by LEDs	Average uncertainty in tube location < 7.5 mm; maximum uncertainty < 13 mm	1975
J. Engel and J. Dagan[82]	Soft tissue stretching via magnetic attraction of a permeable implant	Accommodate bone grafts in reconstruction of congenital deformities	Sm-Co magnet with surface area – 2 cm^2 acts on 1.3 cm diameter steel-ball implant	Skin elongation rate in canine tests was ~ 2.5 mm per day at force of 7 N	1978
J.R. Wolpaw et al. [83,84,85]	Muscle stretching via electromagnetic action on a permeable implant	Assessment of skilled motor activity via muscle stimulation	493-turn coil driven with 0.1 and 3.6 s pulses acts on implanted iron slug	Primate trials demonstrated that muscle stretch affects cortical motor control	1978
A.D. Gruneberger et al. [86,87]	Passive, retropubic magnetic implant closure system	Controlled urethral closure to overcome inconstancy	16-gram, Sm-Co magnet acts to attract auxiliary Sm-Co magnet in a clamping scheme	Animal testing demonstrated incontinence over periods from 10 to 33 weeks.	1983
R.G. Bresier[88]	Magnetic field-based proximity probe with audible signaling	Controlled placement of endotracheal tubes in anesthetized patients	Two field-sensing coils and a differential amplifier form detector input stage	Probe used to monitor endotracheal tube to prevent blockage of bronchial tree	1984

[81] D. J. Cullen, R. S. Newbower, and M. Gemer, Anesthesiology 43, 596(1975).
[82] J. Engel and J. Dagan, The Hand 10, 312 (1978).
[83] J. R. Wolpaw and T. R. Colbum, Brain Res. 141, 193 (1978).
[84] J. R. Wolnaw, Science 203. 465 (1979).
[85] T. R. C&urn; W. Vaughn; J. L. Christensen, and J. R. Wolpaw, Med. Biol. Eng. Comput. 18, 145 (1980).
[86] A. D. Griineberger and G. R. Hennig, J. Urol. 130, 798 (1983).
[87] A. D. Griineberger, G. R. Hennig, and F. Bullemer, J. Biomed. Eng. 6, 102 (1984).
[88] R. G. Bresler, U.S. Patent No. 4 445 501 (1 May 1984).

Table 7. Design and performance characteristics of various exploratory magnetic manipulation systems that are either functionally stereotactic or that employ stereotactic instrumentation in their operation. [89]

Authors	Apparatus/ Method	Application	Manipulated Implant	Results	Year
H.L. Rosomoff[90]	Macpherson stereotacic frame with #15 needle housing magnetic probe	"stereomagnetic" occlusion of intracranial aneurysms	250 mg of particulate iron infused via catheter over a 20-min period	60 min. required for thrombosis	1966
Montgomery et. Al. [91,92]	3 orthogonal pairs of superconducting magnets with air core imaging ports	Blockage of vascular malformations, chemotherapy delivery	0.6-mm Silastic catheter with either Pt-co or iron tip and detachable balloon	Engineering and design study	1969
J.F. Alksne[93,94]	Rand-Wells steotactic frame with a 6-mm diameter permanent – magnet probe	Thrombosis of intracranial aneurysms	Carbonyl iron powder in 25% human serum albumin, passed via the probe into aneurysm	41 patients treated	1972
S.K. Hilal et. Al. [95,96]	Hand-held, 0.4-H, air core ac solenoid for proulsion with bar-magnet steering	Intracranial recording of EEGs, electrothrombosis of aneurysms	Silkastic-tube catheter of ~ 1-mm diam., tipped with radio-opaque Pt-Co magnet	Very strong EEG signals obtained	1974
M.S. Grady et. Al. [97,98]	Manally controlled, water cooled dc electromagnet on 5-axis goniometric mount	Movement of seed along nonlinear paths for forcal RF hyperthermia	Cylindrical Nd-B-Fe magnet 5-mm diam. X 5-mm long, with hemispherical endcaps	Accuracy = ±2 mm in canine brain	1990
R.C. Ritter et. Al. [99,100]	Superconducting multi-coil manipulator, calibration via BRW stereotactic frame	Delivery of various therapies to focal neurological disorders	Nd-B-Fe seed, 3-mm maximum dimension, to tow (eg.) a drug delivery catheter	Apparatus built, testing underway	1992

[89] G.T. Gillies, R.C. Ritter, W.C. Broaddus, M.S. Grady, M.A. Howard III, R.G. McNeil. "Magnetic Manipulation Instrumentation for Medical Physics Research" Rev. Sci.Instrum. 65 (3), March 1994.
[90] H. L. Rosomoff, Trans. Am,Neurol. Assoc. 91, 330 (1966).
[91] B. Montgomery, R. J. Weggel, M. J. Leupold, S. B. Yodh, and R. L. Wright, J. Appl. Phys. 40, 2129 (1969).
[92] D. B. Montgomery, J. R. Hale, N. T. Pierce, and S. B. Yodh, IEEE Trans. Magn. MAGQ 374 (1970).
[93] J. F. Alksne, N. Engl. J. Med. 284, 171 (1971).
[94] J. F. Alksne, Confin. Neurol. 34, 368 (1972).
[95] R. D. Penn, S. K. Hilal, W. J. Michelsen, E. S. Goldensohn, and J. Driller, J. Neurosurg. 38, 239 (1973).
[96] S. K. Hilal, W. J. Michelsen, J. Driller, and E. Leonard, Radiology **113**, 529 (1974).
[97]M. S. Grady, M. A. Howard III, W. C. Broaddus, J. A. Molloy, R. C. Ritter, E. G. Quate, and G. T. Gillies, Neurosurg. **27**, 1010 (1990).
[98] M. S. Grady, M. A. Howard III, J. A. Molloy, R. C. Ritter, E. G. Quate, and G. T. Gillies, Med. Phys. **17**, 405 (1990).

L. Chin[101]	Pairs of coils moved around patient's head, coordinates determined via CRW frame	Delivery of various therapies to focal neurological disorders	Seed designs presently under development	Concept being evaluated	1992

2.2 Stereotaxis, Inc.'s Delivery Strategy

Stereotaxis, Inc. is the leading commercial developer of magnetic stereotaxis systems (MSS) for the medical industry. Examination of their work is important to designing a magnetic guidance system for an untethered magnetic seed and to facilitate knowledge transfer to industry. Table 8 gives an overview of the past generations of MSS reviewed by Stereotaxis. However, discussion in this section will be limited to the most recent generations of MSS.

The first prototype magnetic guidance system was a 6-coil superconducting multicoil helmet built by Wang NMR as a fifth generation device. This device was built for the University of Virginia by Wang NMR and in 1994 characterization of the system was underway in preparation for experimental studies. It was subsequently sold to Stereotaxis Inc. where it developed a leak in 1998, and it is currently warehoused with an estimated cost of approximately $200,000 to fix.[102] Based in part on this prior Wang design, Stereotaxis's primary product is the "TELSTAR" which is shown in Figure 3. It represents the sixth generation of MSS. It uses a 3-coil superconducting system to guide a magnetic tipped catheter throughout the arterial system. There are four current installations for these multi-purpose investigational workstations, which are at Washington University, University of Iowa, Rush-Presbyterian-St. Luke's Medical Center and the University of Oklahoma.

---

[99] M. A. Howard III, M. Mayberg, M. S. Grady, R. C. Ritter, and G. T. Gillies, U.S. Patent No. 5 125 **888** (30 June 1992).
[100] R C Ritter, M. S. Grady M. A. Howard III, and G. T. Gillies, Innov. . . Tech. Biol. Med. 13, **437** (1992).
[101] L. Chin, G. Tang, E. Tang, and M. L. J. Apuzzo, in Scientific Program of the American Association of Neurological Surgeons I992 Annual Meeting, edited by D. 0. Quest (American Association of Neurological Surgeons, Park Ridge, Illinois, 1992), pp. 295-296.
[102] Private telephone communication between the author and Wang NMR.

Table 8. MSS magnetic manipulation systems used to date. [103]

MSS Coil Generation	1	2	3	4	5	6
Coil Type	Wire-wound "Neck-Loop"	Circular Cross-Section Copper-Tubing	Square Cross-Section Copper-Tubing	Superconducting	6-coil Superconducting System	3-coil Superconducting System
Power Supply	Hewlet-Packard 643B (2 each)	Lincwelder DC-250-MK Motor-Generator	Cableform MK-10 Pulse-Modulating Controller and Deep Cycle Batteries	Electronic Measurements EMP-100-200-1211 with Static Bypass Switch	Electronic Measurements EMP-100-200-1211 with Switching Contactors and Supply Drivers	Proprietary
Ramp-Time to Full Current	< 1 s	< 1 s	< 1 s	10 s	300 s	Proprietary
Mounting System	Two-degree Goniometer (Manual)	Hand-Adjustable Cradle	Five-degree Goniometer (Manual)	Four-degree Goniometer (Computerized)	Static Floor-Mounted	Static Floor-Mounted
Protocol for Use	Brain Phantom Gelatin	In vivo	In vivo	Brain Phantom Gelatin	Primates, Human Trials	Human Trials
Dates of Operation	1/87 to 9/87	11/87	7/88 to 8/88	4/90 to 8/90	6/91 to ~95	98-Present

Figure 3. Stereotaxis's TELSTAR Multi-Purpose Investigational Workstation[104]

[103] R.C. Ritter, M.S. Grady, M.D., M.A. Howard III M.D., G.T. Gillies. 'Magnetic stereotaxis: Computer-assisted, image-guided remote movement of implants in the brain'. Innovation et technologie en biologie et mâedecine : Vol. 12, no. 4, p. 444, 1992.

The next generation system that Stereotaxis is focusing on is a more compact and cost effective system, shown in Figure 4, utilizing permanent instead of superconducting magnets. The position of the permanent magnets will be mechanically moved instead of varying current to alter the force on the magnetic tipped catheter.

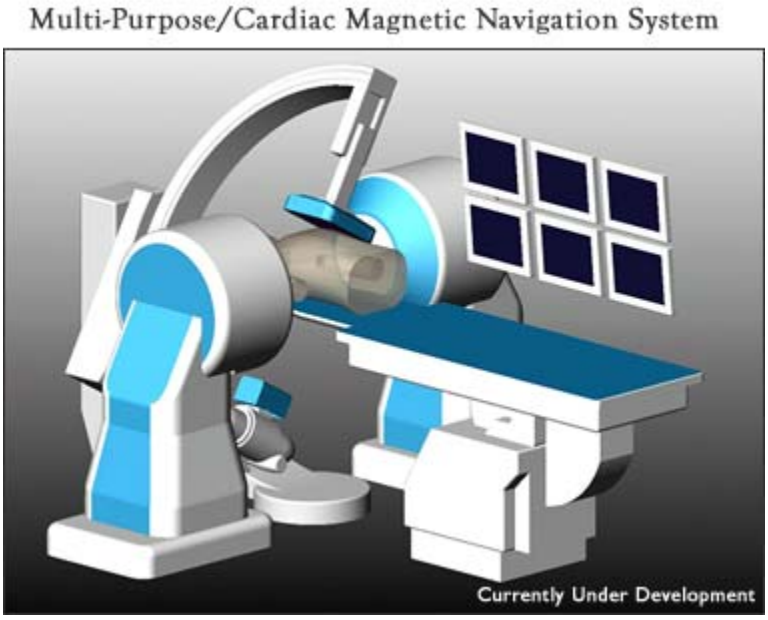

Figure 4. Next Generation of MSS being developed by Stereotaxis, Inc[104]

2.3 FeRx Inc.'s Delivery Strategy

In comparison, FeRx has focused on the use of external permanent magnets and particle transport through tissue. FeRx's strategy has been to use milled 1 μm iron-activated carbon which has a much higher magnetic moment when compared to magnetite. Iron is injected into blood vessels near the target organ and then a single external permanent magnet pulls the particles out of the bloodstream and into the epithelium layers of the organ.

---

[104] Stereotaxis, Inc. http://www.stereotaxis.com, 2002.

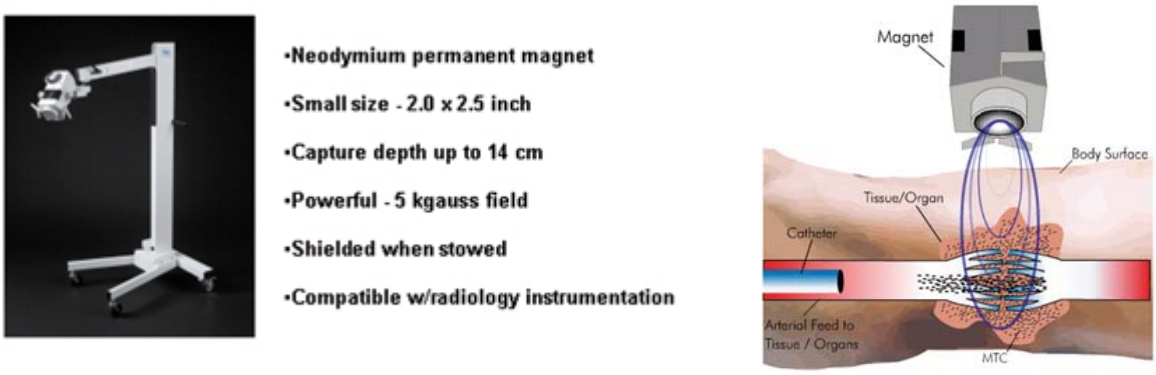

Figure 5. Permanent Magnet and application of magnet used by FeRx[105]

The field is removed from the target organ after approximately 15 minutes and an angiogram is performed to make sure blockage of the main arteries has not occurred. Various drugs are attached to the iron activated carbon depending on the application. This method for drug delivery has been performed for both the liver and bladder.[106] Potential downfalls of this method are the toxicity of the iron, which directly relates to the body's ability to rid itself of excess iron. There is a condition called hemochromatosis in which the liver fails after a slow buildup of too much iron caused by the liver's inability to excrete this waste. Superconducting QUantum Interference Devices (SQUIDS), the most sensitive detector of magnetic flux, have been used to noninvasively determine iron concentration in organs to prevent hemochromatosis.[107] However, FeRx plans to keep the doses in the body under toxic levels by limiting and controlling the amount of infused iron.

---

[105] Jacqueline Johnson, Ph.D. "Magnetic Targeted Carriers: An Innovative Drug Delivery Technology" Magnetics Business & Technology Magazine - Premier Issue 2002. http://www.magneticsmagazine.com/e-prints/FeRx.htm

[106] Jacqueline Johnson, Thomas Kent, Joy Koda, Caryn Peterson, Scott Rudge, Gilles Taposlky "The MTC Technology: A Platform Technology for the Site-Specific Delivery of Pharmaceutical Agents." Fourth International Conference on the Scientific and Clinical Applications of Magnetic Carriers. 22-25, 2002.

[107] Elliot Vichinsky M.D. Transfusion Therapy in Sickle Cell Disease. Oakland Children's Hospital Oakland, California http://sickle.bwh.harvard.edu/transfusion.html

In summary, there have been many uses of magnetic particle manipulation in the human body. However, a single system has yet to emerge that combines the techniques presented into a simple tool with a wide range of applications extensively used by the medical community.

Chapter 3: Modeling

This section describes the controlling variables and their interactions in closer detail. Assumptions about the blood properties, hemodynamic flow conditions, and other mechanical effects are made here in order to simplify the analysis of *in vivo* magnetic guidance.

3.1 Blood Properties

It is important to closely model blood and blood flow in order to engineer an effective magnetic targeted drug delivery system. Blood consists of plasma, which normally occupies approximately 55% by volume of the blood, red cells, white cells and platelets. The red cells are the most numerous and largest, therefore dominating the mechanical properties of blood. They are flexible disks of approximately 8 μm diameter with a thickness ranging from 1-3 μm. White cells are similar in size, but are less abundant compared to the red cells (i.e. 1-2 per 1000 red cells), and they are therefore dynamically negligible. Platelets number 80-100 per 1000 red cells but are small, round cells with diameters of 2-4 μm. The platelets' effects are negligible due to their size and density in the blood. The plasma consists of a solution of larger molecules, but on the scales of motion and at the rates of shear normally encountered in the blood vessels, it can be regarded as a homogeneous Newtonian fluid[108] of viscosity[109] 0.0012-0.0016 kg/(m•s) at 37 °C.

Whole blood cannot be regarded as a Newtonian fluid in blood vessels smaller than 100 μm. Blood also behaves as a shear-thinning fluid whose viscosity varies as a function of

---

[108] A Newtonian fluid is one in which the viscosity coefficient (v) is independent of the velocity gradient

[109] T.J. Pedley, "The fluid mechanics of large blood vessels," Cambridge University Press, Cambridge, 1980.

shear rate. It is suggested by T.J. Pedley that blood can be considered as a Newtonian fluid when the shear rate ***S*** is greater than 100 s^{-1} (i.e. the viscosity is independent of the shear rate). Blood viscosity as a function of shear rate is relatively constant at this limit as illustrated by Figure 6.

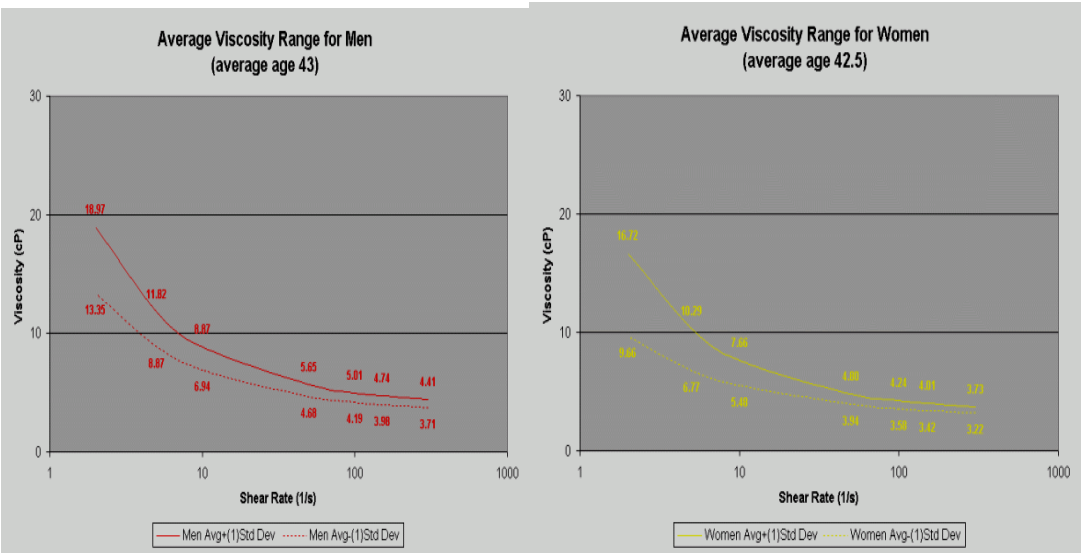

Figure 6. Blood viscosity for men and women with a +/- one standard deviation [110•]

This is, however, only true in the regions of the vessel close to the walls. This is in contrast to the central portion of larger vessels where the velocity profile is nearly uniform and the shear rate is low. Flow in larger blood vessels is more uniform, termed "plug" flow, while in smaller blood vessels the flow front shape is more parabolic (Figure 7).

---

[110] **Rheologics, Inc**. 2001. http://www.rheologics.com/charts.htm

• **Note: Viscosity has units of mass/length-time. Poise is the cgs unit of absolute viscosity in g/cm-sec. To convert from poise to kg/m-sec, divide by 10.**

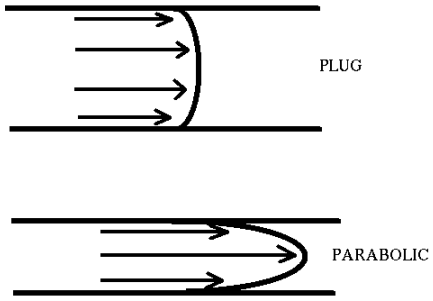

Figure 7. Comparison of plug vs parabolic flow of blood in large and small vessels, respectively.

3.2 Hemodynamic Flow Conditions

Considering the constraints at hand, the calculations that follow are only valid down to vessels with internal diameters smaller than the carotid artery (approximately 0.6 cm) but greater than the arteriole system (approximately 10μm-80 μm). If we consider the worst case (i.e., in the carotid), the mean lumen diameter (internal diameter of the blood vessel) is 0.6 cm and a measured velocity profile with time is illustrated in Figure 8. Here we see that the velocity ranges from about 10 to 65 cm/s.

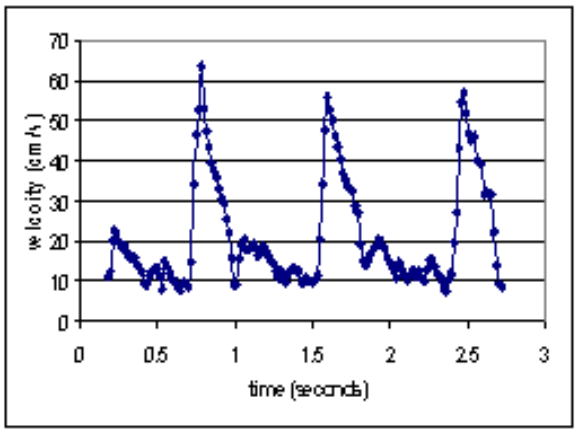

Figure 8. Blood flow in a human carotid artery. [111]

---

[111] Jane F. Utting. **Measurement of Regional Cerebral Blood Flow using MRI**. University College London. Department of Medical Physics & Bioengineering. http://www.medphys.ucl.ac.uk/posters99/jfupstr/sld007.htm

When the particle size is less then 100 μm and flow velocities are on the order of μm/s or less, the Reynolds number (Re)[112,113] is often less then one. Here,

$$\mathrm{Re} = \frac{\rho U d}{\mu}, \tag{5}$$

where ρ is the density of the fluid, U is the free stream velocity, μ is the absolute or dynamic viscosity, and d is the diameter of the sphere. When the Reynolds number is this low, forces experienced by the particle are governed primarily by inertial forces. Under such conditions, the viscous force at low Reynolds numbers is governed by Stokes Law,

$$F = 6\,\pi\,\eta\,v\,r, \tag{6}$$

where η is the viscosity of blood, about 0.004 kg/(m*s), v is the relative velocity of the fluid, and r is the radius. The flow force is non-stationary (Figure 8), so in general is more complicated than the simple model shown. However, this model holds at low flow rates, e.g. in the capillaries.

3.3 Comparison of Hemodynamic Forces with Magnetic Forces

The magnetic force exerted on the microsphere is governed by electromagnetic field and constitutive relationships. Maxwell's four equations describe most electromagnetic phenomenon. They are composed of Faraday's law, Gauss's law, a generalization of Ampère's law, and a statement of the nonexistence of magnetic monopoles.

Faraday's law is based on the experimental determination that a time-changing magnetic flux induces an electromotive force.

$$\oint_C \bar{\xi} \bullet d\mathrm{l} = -\int_S \frac{\partial \bar{\beta}}{\partial t} \bullet ds \qquad \nabla \mathrm{x} \bar{\xi} = -\frac{\partial \bar{\beta}}{\partial t} \tag{7}$$

---

[112] E.M. Purcell. "Life at Low Reynolds Number" Lyman Laboratory, Harvard University, Cambridge, Mass 02138. June 1976. http://brodylab.eng.uci.edu/~jpbrody/reynolds/lowpurcell.html

[113] Brody, Austin, Goldstein, & Yager. "Biotechnology at Low Reynolds Numbers" Biophysical Journal, Dec 1996. http://publish.aps.org/eprint/gateway/eplist/aps1996jul26_001

where curve C encloses surface S.

Gauss's law is based upon Coulomb's law and experimental determination that electric charges attract or repel one another with a force inversely proportional to the square of the distance between them.

$$\int_S \overline{D} \bullet ds = \int_V \rho \ \mathrm{dv} \ , \qquad \nabla \bullet \overline{\mathrm{D}} = \rho \tag{8}$$

where surface S encloses the volume V.

Ampère's law states that the line integral of the magnetic field over any closed curve must equal the total current enclosed by that curve and that the time-varying electric fields produce magnetic fields.

$$\int_C \overline{H} \bullet dl = \int_S \overline{J} \bullet ds + \int_S \frac{\partial \overline{D}}{\partial t} \bullet ds \ , \qquad \nabla \ \mathrm{x} \ \overline{H} = \overline{J} + \frac{\partial \overline{D}}{\partial t} \tag{9}$$

where curve C encloses surface S.

Maxwell's final equation states that no magnetic monopoles exist and that all magnetic field lines always close on themselves.

$$\oint_S \overline{B} \bullet ds = 0 \ , \qquad \nabla \bullet \overline{B} = 0 \tag{10}$$

where the surface S encloses a volume V.

The force due to a gradient in a magnetic field is a reduction of the Lorentz force.[114] The Lorentz force $\vec{F} = \int dv \, \vec{J}(\vec{r}) \ \mathrm{x} \ \vec{B}(\vec{r})$ for the case that magnetic flux density $\vec{B}$ varies slowly over the extent of the current. We can then expand

$$B_i(\vec{r}) = B_i(0) + \vec{r} \bullet (\vec{\nabla} B_i)_{\vec{r}=o} + \ldots \ , \tag{11}$$

---

[114] Discussion with David de Wolf. Electrical and Computer Engineering Department of Virginia Tech. 2002.

which we can write more succinctly as

$$B_i(\vec{r}) = B_i(0) + (\vec{r} \bullet \nabla) B_i(0) + \ldots \tag{12}$$

In the understanding that the gradient operates first on the B-field before we set $\vec{r} = 0$. If we ignore higher-order expansion terms in (11) and (12), then $\vec{F} = \vec{F}_a + \vec{F}_b$ with

$$\begin{aligned} &\vec{B}_o \equiv \vec{B}(r)\big|_{r=0} \\ &\vec{B}' \equiv \vec{r} \bullet (\vec{\nabla} B_i + \vec{\nabla} B_j + \vec{\nabla} B_k) \\ &\vec{F}_a = \int dv \vec{J}(\vec{r}) x \vec{B}_o, \text{ and } \vec{F}_b = \int dv \vec{J}(\vec{r}) \vec{B}' \end{aligned} \tag{13}$$

We show that $\vec{F}_a = 0$ by showing that $\int dv \vec{J}(\vec{r}) = 0$. That follows from the following theorem which holds for any two function $f(\vec{r})$ and g($\vec{r}$) if $\vec{\nabla} \bullet \vec{J} = 0$:

$$\int dv [f\ \vec{J} \bullet \vec{\nabla} g - g\ \vec{J} \bullet \vec{\nabla} f] = 0 \tag{14}$$

The theorem is proved by doing an integration by parts of either the first or the second term, using the fact that $\vec{J}(\vec{r}_s) = 0$ at boundary-surface locations, and applied only under the stationary-current condition, $\vec{\nabla} \bullet \vec{J} = 0$.

If we set f = 1 and $g = x_i$ in (14). That tells you that $\int dv\, J_i(\vec{r}) = 0$ and therefore that $\int dv\, \vec{J}(\vec{r}) = 0$, which is what was needed to prove that $\vec{F}_a = 0$. To find a useful form for $\vec{F}_b$ is considerably more difficult, at any rate we now have

$$\vec{F} = \vec{F}_b = \int dv\, \vec{J}(\vec{r}) \text{ x } (\vec{r} \bullet \vec{\nabla}) \vec{B}_o \tag{15}$$

Consider the x_1 component of this:

$$\begin{aligned} F_1 &= \int dv [J_2 (\vec{r} \bullet \vec{\nabla}) B_{o3} - J_3 (\vec{r} \bullet \vec{\nabla}) B_{o2}] \\ &= \sum_j \int dv [J_2 (x_j \frac{\partial B_{o3}}{\partial x_j}) - J_3 (x_j \frac{\partial B_{o2}}{\partial x_j})] \end{aligned} \tag{16}$$

This is more easily handled when we write it as

$$F_1 = \sum_j \frac{\partial B_{03}}{\partial x_j} \int dv\ x_j\ J_2 - \sum_j \frac{\partial B_{02}}{\partial x_j} \int dv\ x_j\ J_3 \tag{17}$$

To make this into a form into which we can introduce the magnetic dipole moment

$$\vec{m} \equiv \frac{1}{2}\int dv\ \vec{r} \times \vec{J}(\vec{r}) \tag{18}$$

we make the replacement

$$\int dv\ x_j J_k = \frac{1}{2}\int dv(x_j J_k + x_k J_j) + \frac{1}{2}\int dv(x_j J_k - x_k J_j) \tag{19}$$

noting that the first integral is zero, as follows from (14) by setting $f = x_j$ and $g = x_k$ so that

$$\int dv\ x_j J_k = \frac{1}{2}\int dv(x_j J_k - x_k J_j) = \pm\frac{1}{2}\int dv(\vec{r} \times \vec{J})_i \tag{20}$$

where i,j,k is either a right-handed (+ sign) or a left handed (- sign) permutation of 1, 2, 3. Equation (17) now becomes

$$F_1 = \frac{1}{2}\sum_j \frac{\partial B_{03}}{\partial x_j}\int dv\ (x_j J_2 - x_2 J_j) - \sum_j \frac{\partial B_{02}}{\partial x_j}\int dv\ (x_j J_3 - x_3 J_j) \tag{21}$$

Completing the sum over all possible j we get 4 terms:

$$F_1 = \frac{\partial B_{03}}{\partial x_1}\int dv(\vec{r} \times \vec{J})_3 - \frac{\partial B_{03}}{\partial x_3}\int dv(\vec{r} \times \vec{J})_1 + \frac{1}{2}\frac{\partial B_{02}}{\partial x_1}\int dv(\vec{r} \times \vec{J})_2 - \frac{1}{2}\frac{\partial B_{02}}{\partial x_2}\int dv(\vec{r} \times \vec{J})_1 \tag{22}$$

or, in terms of components of the magnetic dipole moment:

$$F_1 = m_3\frac{\partial B_{03}}{\partial x_1} - m_1\frac{\partial B_{03}}{\partial x_3} + m_2\frac{\partial B_{02}}{\partial x_1} - m_1\frac{\partial B_{02}}{\partial x_2} \tag{23}$$

which is more succinctly written as

$$F_1 = (\vec{m} \times \vec{\nabla})_2 B_{03} - (\vec{m} \times \vec{\nabla})_3 B_{02} = [(\vec{m} \times \vec{\nabla}) \times \vec{B}_o]_1 \tag{24}$$

Doing the same for the other two components of F we find

$$F = (\vec{m} \times \vec{\nabla}) \times B_o \tag{25}$$

This can be simplified because $\vec{m}$ is a constant vector. In simplified derivative notation:

$$\begin{aligned} F_1 &= (m_3\partial_1 - m_1\partial_3)B_{03} - (m_1\partial_2 - m_2\partial_1)B_{02} \\ &= (m_3\partial_1 B_{03} - m_1\partial_3 B_{03}) - (m_1\partial_2 B_{02} - m_2\partial_1 B_{02}) \\ &= \vec{m} \bullet \partial_1\vec{B} - m_1\vec{\nabla} \bullet \vec{B} \end{aligned} \tag{26}$$

The last term is zero (Maxwell's equation). Hence also

$$\vec{F} = \sum_{i=1}^{3} \hat{x}_i(\vec{m} \bullet \frac{\partial \vec{B}_o}{\partial x_i}) \tag{27}$$

or, using the fact that $\vec{m}$ is a constant,

$$\vec{F} = \vec{\nabla}(\vec{m} \bullet \vec{B}_o) \tag{28}$$

As before, the derivative at $\vec{r}$ needs to be taken first before setting $\vec{r} = 0$.

As a check we consider a current loop in the $z = 0$ plane. The magnetic dipole moment here is $\vec{m} = (I\pi r^2)\hat{z}$ if r is the radius of the loop. The Lorentz force is now

$$\vec{F} = \oint I \; d\vec{l} \times \vec{B} \tag{29}$$

so that the gradient force is

$$\vec{F} = \vec{F}_b = I \oint d\vec{l} \times (\vec{r} \bullet \vec{\nabla}) \vec{B}_o \tag{30}$$

with the auxiliary definitions:

$$\begin{aligned} d\vec{l} &= (r d\varphi)\hat{\varphi} \\ \vec{r} &= \hat{x}\cos\varphi + \hat{y}\sin\varphi \\ \hat{\varphi} &= -\hat{x}\sin\varphi + \hat{y}\cos\varphi \end{aligned} \tag{31}$$

This transforms into

$$\begin{aligned} \vec{F} &= Ir^2 \int_0^{2\pi} d\varphi(-\hat{x}\sin\varphi + \hat{y}\cos\varphi) \times (\cos\varphi \frac{\partial \vec{B}}{\partial x} + \sin\varphi \frac{\partial \vec{B}}{\partial y})_0 \\ &= (I\pi r^2)[-\hat{x} \times \frac{\partial \vec{B}}{\partial y} + \hat{y} \times \frac{\partial \vec{B}}{\partial x}] \\ &= m[-\hat{z}\frac{\partial B_y}{\partial y} + \hat{y}\frac{\partial B_z}{\partial y} - \hat{z}\frac{\partial B_x}{\partial x} + \hat{x}\frac{\partial B_z}{\partial x}] \\ &= m\sum_{i=1}^{3} \hat{x}_i \frac{\partial B_z}{\partial x_i} - \vec{m}\vec{\nabla} \bullet \vec{B} \end{aligned} \tag{32}$$

Again, the last term is zero (Maxwell's equation) so that as in (27) and (28) we again find

$$\vec{F} = m\sum_{i=1}^{3} \hat{x}_i \frac{\partial B_z}{\partial x_i} = \sum_{i=1}^{3} \hat{x}_i (\vec{m} \bullet \frac{\partial B_o}{\partial x_i}) \tag{33}$$

We will use this result to model the force experienced by magnetic microspheres synthesized by Dr. Judy Riffle's research group. In order to calculate the moment of the magnetic microspheres we will examine the present experimental results obtained by Dr. Judy Riffle's research group in the Department of Chemistry at Virginia Tech. They have successfully synthesized magnetite nanoparticles in 2000 and 5000 g/mol

polyethylene oxide. The saturation magnetization of the samples is approximately 20 emu/g (per gram of sample, not per gram of magnetite). It is assumed this can be increased to at least 30 emu/g and that polylactide can be used as the stabilizer. This would yield 2 μm polylactide microspheres with a maximum saturation magnetization of about 30 emu/g. For our field design, if we assume the density of magnetite is 5 g/cm^3 and the density of PEO is 1 g/cm^3, then at 30 emu/g of material, this is approximately 45 weight percent nanomagnetite. Then if we have 45 g magnetite at a density of 5 g/cm^3 it has a volume of 9 cm^3. Thus 55 g PEO at 1 g/cm^3 is 55 cm^3 of PEO. Therefore, we have (45 + 55)g/(9 + 55)cm^3 which equals an overall particle density of 1.56 g/cm^3.

Multiplying the 30 emu/g saturation magnetization by the 1.56g/cm^3 density gives 47 emu/cm^3 (at saturation) in Gaussian units. Multiplying by 1000 converts the magnetization to SI units, 47000 A/m. We then calculate the volume for a sphere of 2 μm diameter.

$$V=\frac{4}{3}\pi r^3 \qquad (34)$$

This gives a volume of 3.35 x 10^{-17} m^3 and multiplying this by the moment of the particle is (47000 A/m)(3.35 x 10^{-17} m^3) = 1.57 x 10^{-12} A-m^2.

For a source magnet having a field of 0.5 T, these particles will be essentially saturated, i.e. completely aligned, at body temperature. Therefore, in a gradient of 1 Tesla/meter, the moment is multiplied by the gradient for the magnetic force, which is in the direction of the field.

A magnetic force of 1.57 x 10^{-12} A-m^2 * 1 T/m = 1.51 x 10^{-12} N. [¥]

[¥] 1 Tesla = 1 kg/A-sec^2 and 1 Newton = 1 kg-m/sec^2

It is assumed that the particle should be held stationary in the flow. Using Stokes Law the maximum drag force is calculated to be 0.00001 m/s and 0.000002 m/s for a viscosity of 0.004 and 0.02 kg/(m•s), respectively.

The magnetic force is a function of the volume (r^3) of the particle and the hemodynamic drag force is a function the radius (r^1). If the magnetic force on the particle is balanced with the hemodynamic drag force as a function of particle radius at various free stream velocities U, the crossovers correspond to points of force equilibrium. These conditions are located at 4.5, 6.4 and 15 μm at velocities of 0.00005, 0.0001, and 0.0005 m/s (Figure 9) for a viscosity of 0.004 kg/(m•s). This calculation provides additional information for selecting field gradients, particle size, and the required magnetic moments of the particles.

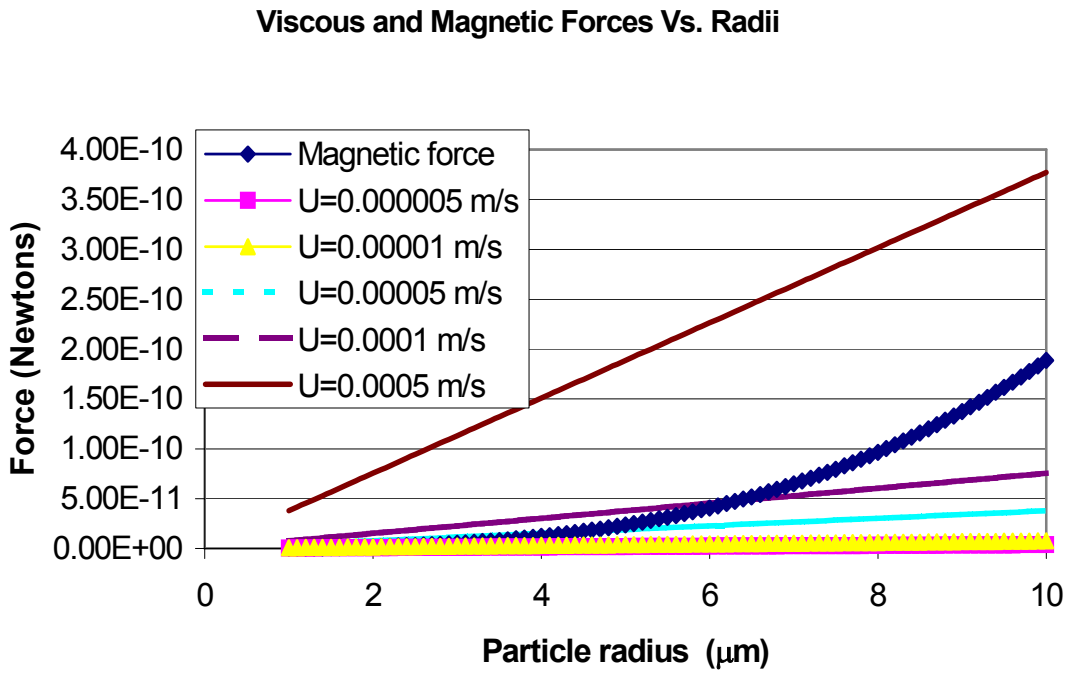

Figure 9. Magnetic and hemodynamic drag forces as a function of particle radius[115]

[115] Courtesy of Dr. Jack Lesko, ESM Department of Virginia Tech.

The capillary flow is approximately 0.00047 m/s[116] and their size decreases to ~15 μm. Therefore an approximately 15 μm diameter magnetite microsphere would be able to maneuver around most of the capillaries. For the worst case scenario of the full systolic flow in the artery at 0.7 m/s a 600 μm particle would be needed for stopping the particle in flow. Comparing different materials gives an additional feel for which parameters should be most closely controlled. The increase of the moment of the magnetic seed decreases the needed particle size of the particle to resist the same flow. Therefore, an increase of moment to 300 emu/g gives a minimum particle size of 5 μm compared to a 15 μm microsphere of magnetite at 0.0005 m/s (flow experienced in the capillaries).

3.4 Other Mechanical Effects

Other mechanical effects also affect guidance. These include tissue porosity and the allowable cell damage for a given procedure. The amount of magnetic force needed to pull a particle out of flow can be significantly less then the magnetic force needed to counteract the drag forces in a stream. FeRx, Inc. is exclusively basing their delivery strategy on this effect.

---

[116] M. Stücker, V. Baier, T.Reuther, K. Hoffmann, K. Kellam and P. Altmayer, "Capillary Blood Cell Velocity in Human Skin Capillaries Located Perpendiculary to the Skin Surface: Measured by a new Laser Doppler Anemometer," Microvascular Research 52, 188-192 (1996). (http://www.lawrenz.com/cam1lit2.htm)

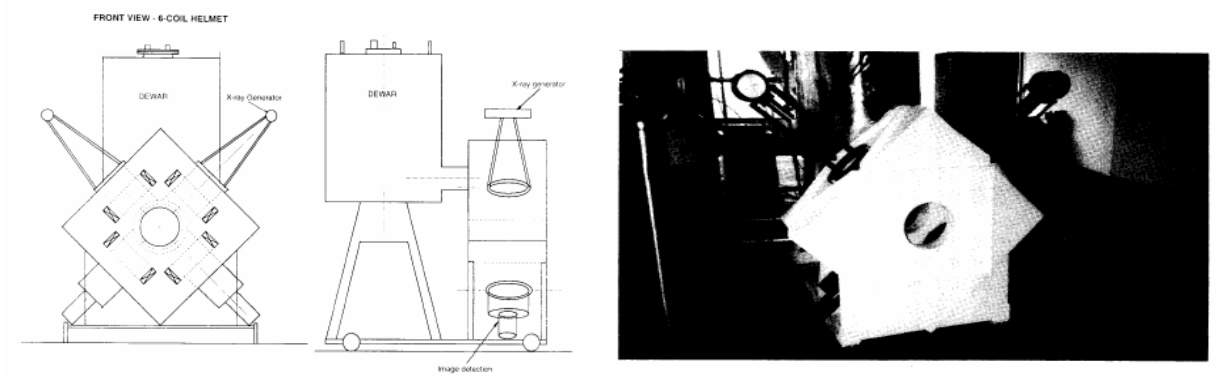

Figure 10. 6-coil super-conducting MSS built by Wang NMR, Inc. [117]

One of the most advanced MSS systems built to date is the system shown in Figure 10. There are multiple justifications for using this system or a modified version of it. The 6-coil system has some advantages that can be seen over the current TELSTAR system in that it has a relatively large field-gradient product that is attainable over an area of approximately 20 cm and has more complete control in all three degrees of freedom. The calculations shown in Figure 11 are derived from a single coil. Examining this data it is evident that a gradient of 12 T/m and a field over 1.5 T is present at a distance of 10 cm from the coil midplane. Rogers Ritter also showed using the other 5 coils to shape the field and gradients will result in higher gradients, faster ramp times, and increased control of the magnetic seed. The use of all 6 coils simultaneously allowed the respective fields and gradients to superposition and significantly increasing the field and gradient in the manipulation space compared to the use of a singular coil. This therefore allowed increased control of the magnetic seed.

---

[117] Robert G. Mcneil, Rogers C. Ritter, Bert Wang, Michael A. Lawson, George T. Gillies, Kevin G. Wika, Elizabeth G. Quate, Matthew A. Howard III, and M Sean Grady. "Functional Design Features and Initial Performance Characterisitcs of a Magnetic-Implant Guidance System for Stereotactic Neurosurgery." IEEE Transactions on Biomedical Engineering. Vol. 42. No. 8. August 1995.

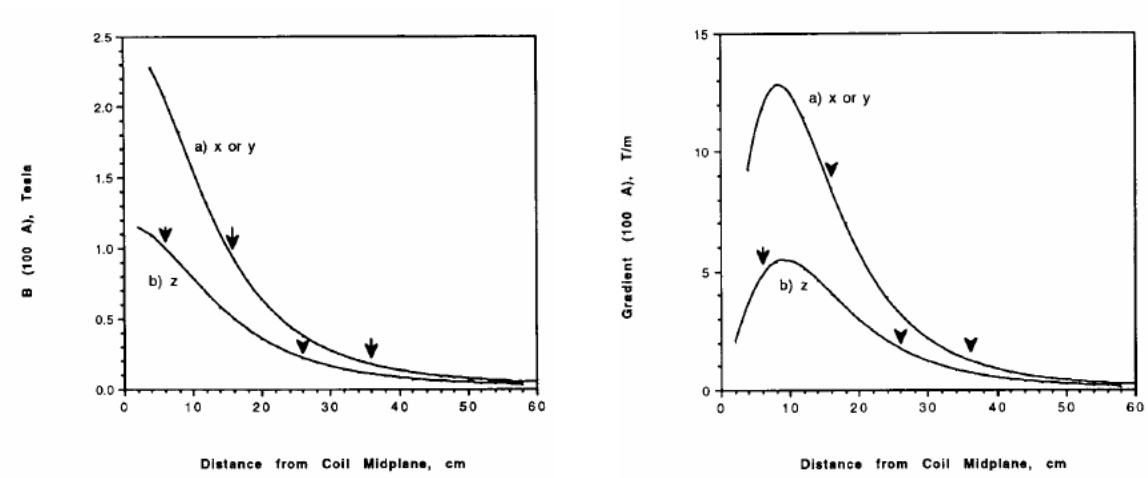

Figure 11. Calculated field and gradients along the axis for (a) x or y-axis coil, and (b) z-axis coil for 6-coil superconducting system. The arrows indicate the edge of a 20-cm diameter sphere centered in the region where a head can be located. [117]

Using the 6-coil MSS system we will assume we are operating at a 10 T/m gradient and that the material is in saturation. Only a 200 μm magnetite microsphere is needed to counteract the full arterial flow at 0.7 m/s and a 4.6 um particle for capillary flow at 0.0005 m/s.

Specifically the assumptions made in this section are the simplification of blood to an average viscosity, a stationary flow force, and low flow rates such as found in the capillaries. Other assumptions that are made are the maximum field and gradient that can be obtained due to cost restraints.

Chapter 4: Experimental

This section discusses the design and construction of a magnetic particle guidance system. The maximum fields and gradients for this system and thus its overall design were restricted primarily by cost restraints. This system was then modeled using Ansoft's 3D Electromagnetic Finite Element Analysis software and compared to measured values from a Hall probe. The drug delivery vehicle, a magnetic seed, was characterized using a vibrating sample magnetometer in order to predict a desired response. Finally, the magnetic seed was investigated under various flow conditions *in vitro* to analyze the effectiveness of the drug delivery system.

4.1 Design and Construction of a Magnetic Microsphere Guidance System

A system was designed for laboratory analysis of magnetic particle guidance. Design assistance was obtained from Dr. Rogers Ritter and Dr. Duke Creighton at Stereotaxis Inc. to build a system with a variable field and gradient. Magnet Sales & Manufacturing Inc. was contracted to construct a variable field and gradient NdFeB permanent magnet system to the designed specifications.

Integrated Motion was contracted to build in parallel a non-ferric frame, motors, and controllers to vary the field and gradient over a set area. The motors were designed to withstand non-linear forces experienced by the magnets with a calculated maximum pull of 500 lbs per magnet. A minimum separation of 0.5 inches was ensured between the field magnets. The system had a variable field and gradient from 0-0.5T and 0-13 T/m respectively over a range of volumes.

Design and construction of an improved magnetic microsphere investigation system was completed (Figure 12). The frame was made of extruded aluminum and bolted to a lab bench for structural stability. The actuators used were WM60 Precision Technology

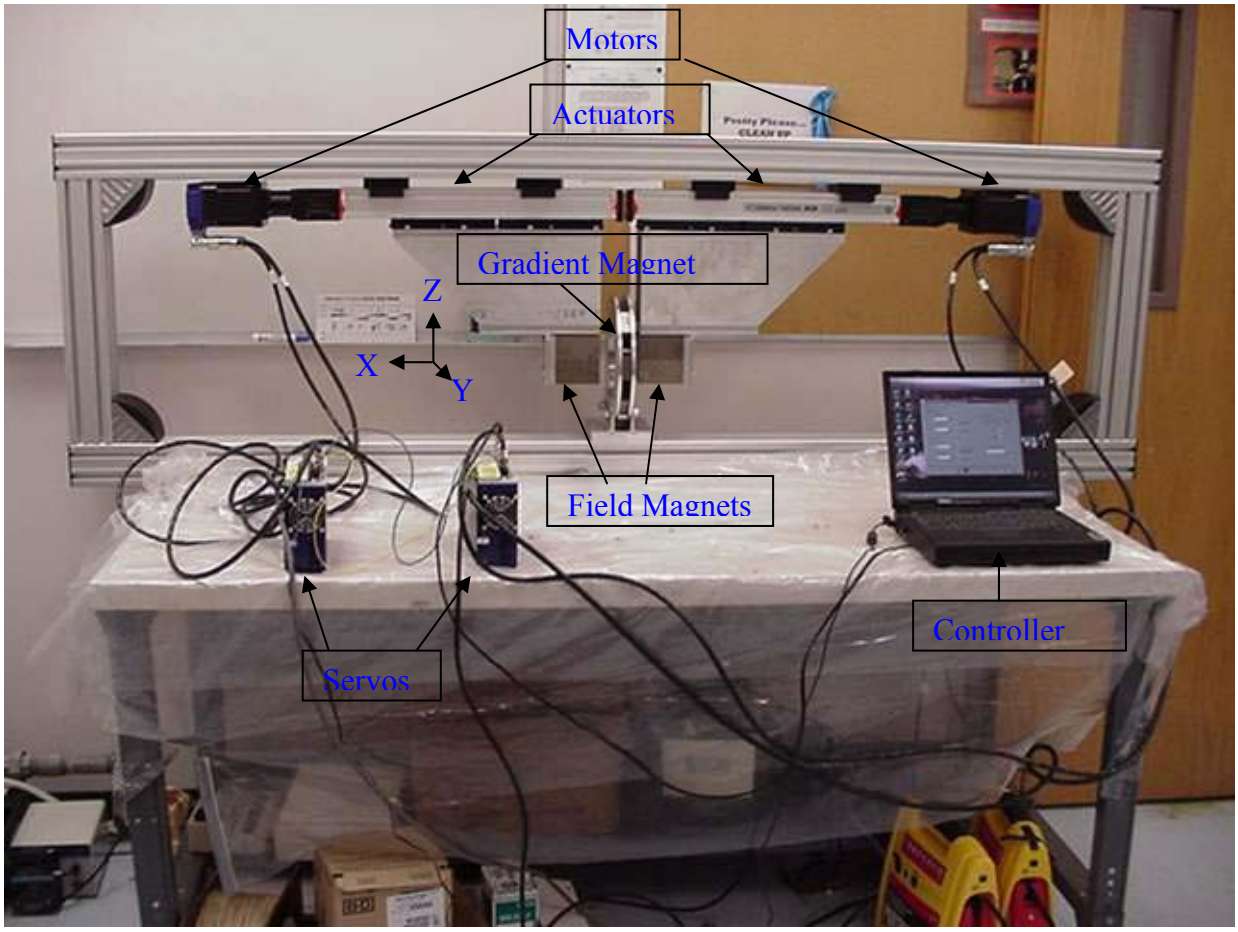

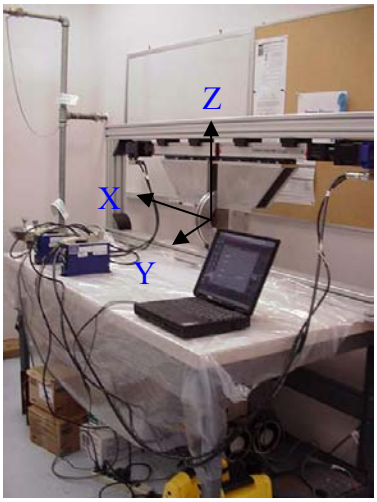

Figure 12. Variable magnetic field and gradient test system.

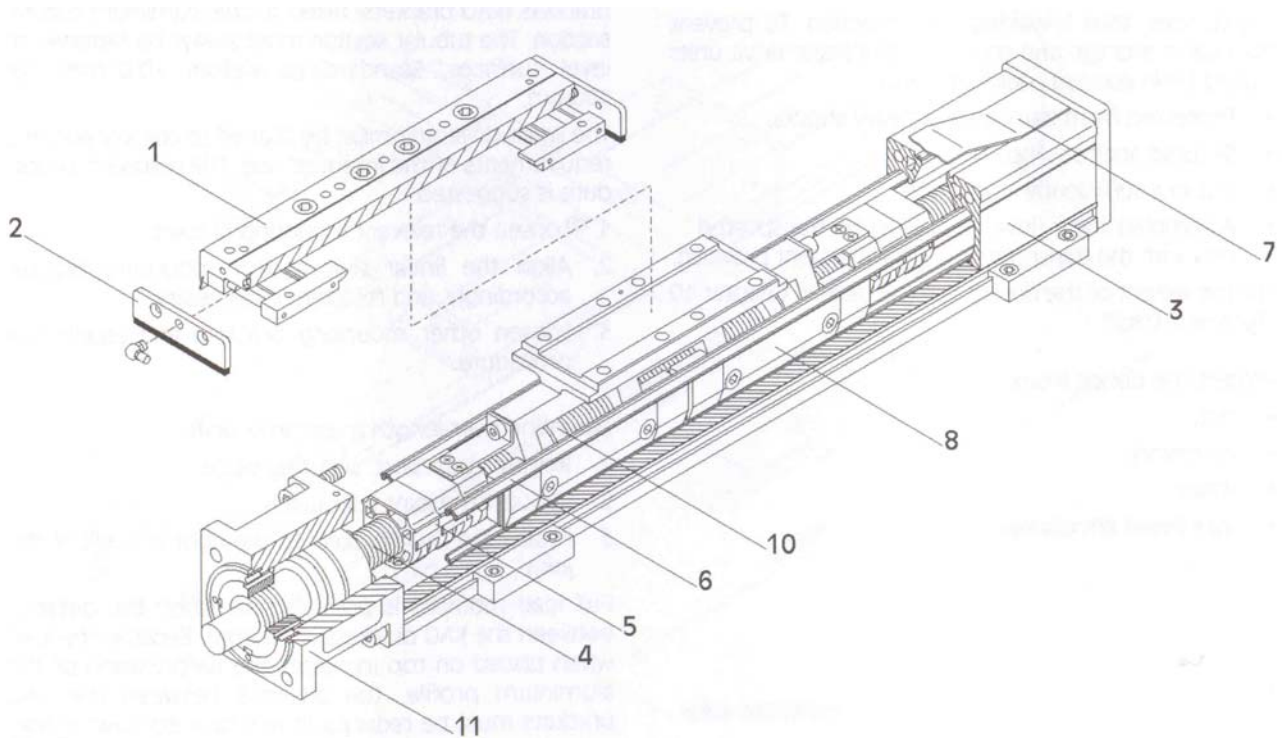

Figure 13. Wiesel Powerline WM60 Actuator. The actuator consists of a sliding carriage(1), scraper brushes(2), tubular section with sliding bars(3), ball screw(4), guideway for screw supports(5), guideways(6), covering strip(7), ball-bearing guided carriage(8), ball nut unit(10), bearing housing and fixed bearing(11).[118]

Wiesel Powerline that had a 100 mm travel with a 650 mm total length (Figure 13). The motors used were Goldline XT with 1.81 lb-ft continuous torque at stall, 4.35 lb-ft peak torque at stall, maximum speed of 6000 rpm, brushless servo motors with single speed resolver (Figure 14). The servos used were a Servostar brushless servo amplifier with integrated power supply rated at 3 amps continuous power (Figure 15).

The original system's magnets that Stereotaxis used were relatively free moving compared with the improved system. This allowed a maximum field of 0.1T and a gradient of 1 T/m. In the original system developed at Stereotaxis if the end field magnets were moved closer together in order to increase the field and gradient, also

[118] Wiesel Powerline Product Literature. NEFF Antriebstechnik Automation GmbH. April 1, 2002.

decreasing the available workspace, the magnets would overcome the small frictional forces that were present and become lodged together. A higher field and gradient with the addition of motors and actuators allowed the magnets to be moved closer together and resist the attractive forces of the magnet. The variable magnetic field and gradient test system allows us to achieve high fields and gradients with a large workspace. The large magnetic workspace also allows us to in the future visually monitor the microspheres using a microscope equipped with long working distance objectives.

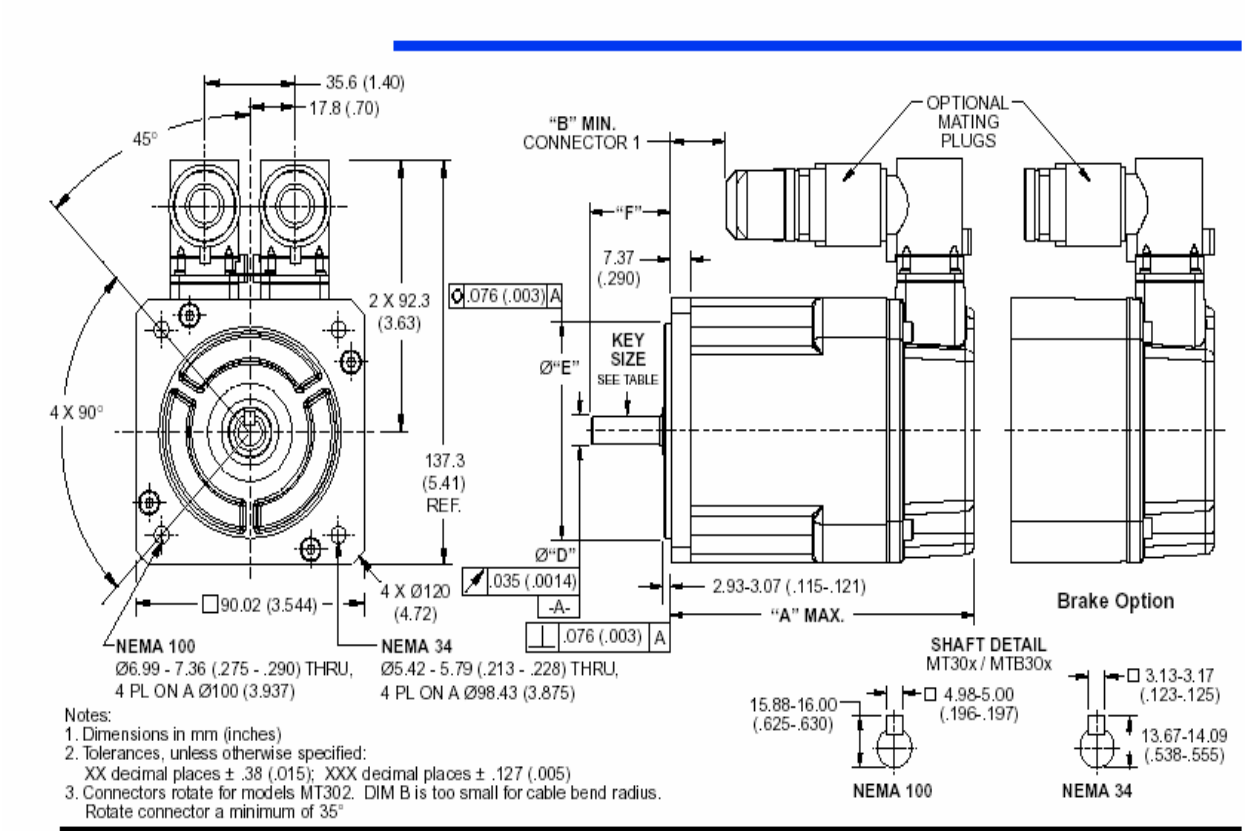

Model	"A" MAX.		"B" MIN.		"D"		"E"		"F" ±.76 (±.030)		Key Length	
	with brake	without brake	with brake	without brake	NEMA 34	NEMA 100	NEMA 34	NEMA 100	NEMA 34	NEMA 100	NEMA 34	NEMA 100
MT(B)302	165.6 (6.520)	120.1 (4.730)	65.14 (2.565)	19.93 (.785)	9.512-9.525	14.01	73.05	80.03			no	20 (.79)
MT(B)304	183.1 (7.210)	137.7 (5.420)	82.67 (3.255)	37.46 (1.475)	(.3745-.3750)	13.99	73.00	79.99	31.75	30	keyway	20 (.79)
MT(B)306	198.6 (7.820)	153.2 (6.030)	98.16 (3.865)	52.95 (2.085)	12.69-12.70	(.5515	(2.876	(3.151	(1.250)	(1.181)	19 (.75)	20 (.79)
MT(B)308	231.7 (9.120)	186.2 (7.330)	131.2 (5.165)	85.97 (3.385)	(.4995-.5000)	.5511)	2.874)	3.149)			19 (.75)	20 (.79)

Figure 14. Diagram of Goldline XT MT(B)304 Motor.[119]

[119] Kollmorgen GOLDLINETM XT Brushless Series Motors -30 Frame Size. Product Literature. 2002.

Figure 15. Servostar brushless servo amplifier with integrated power supply.

A laptop was used as a controller interfaced by a RS-232 port to the system's actuators. Kollmorgen's Servostar software running on the laptop was used to program the actuators. The field magnets position, velocity, and the timing of their movement can be controlled directly through the software (Figure 16).

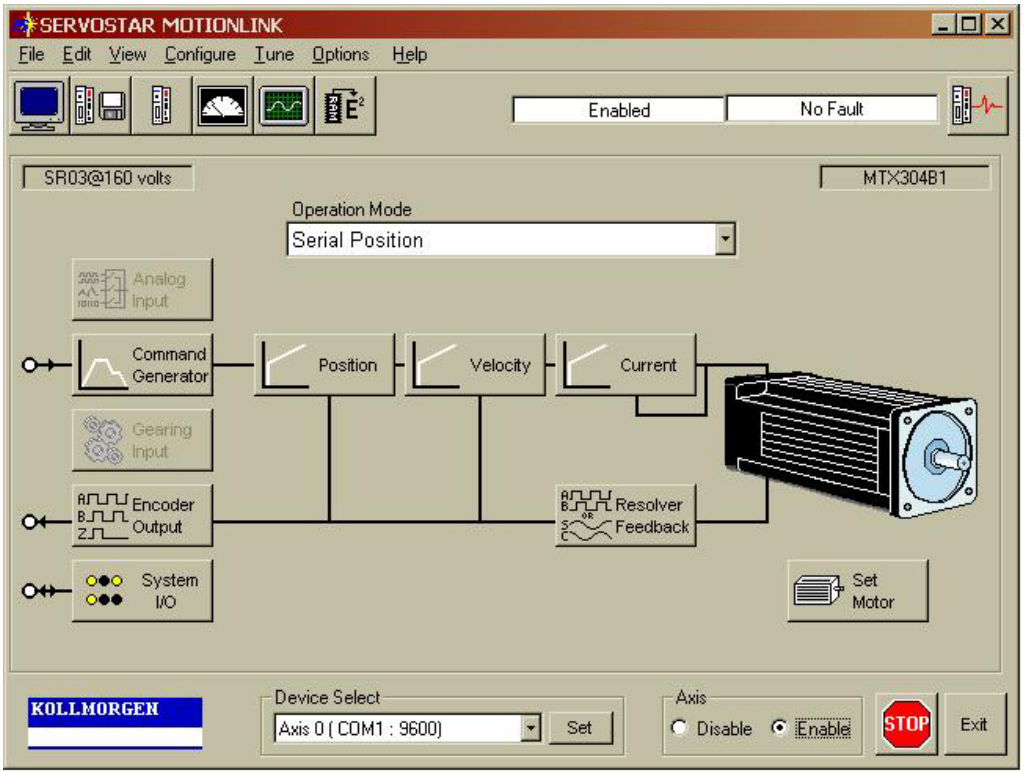

Figure 16. Kollmorgen's Servostar Motionlink software.

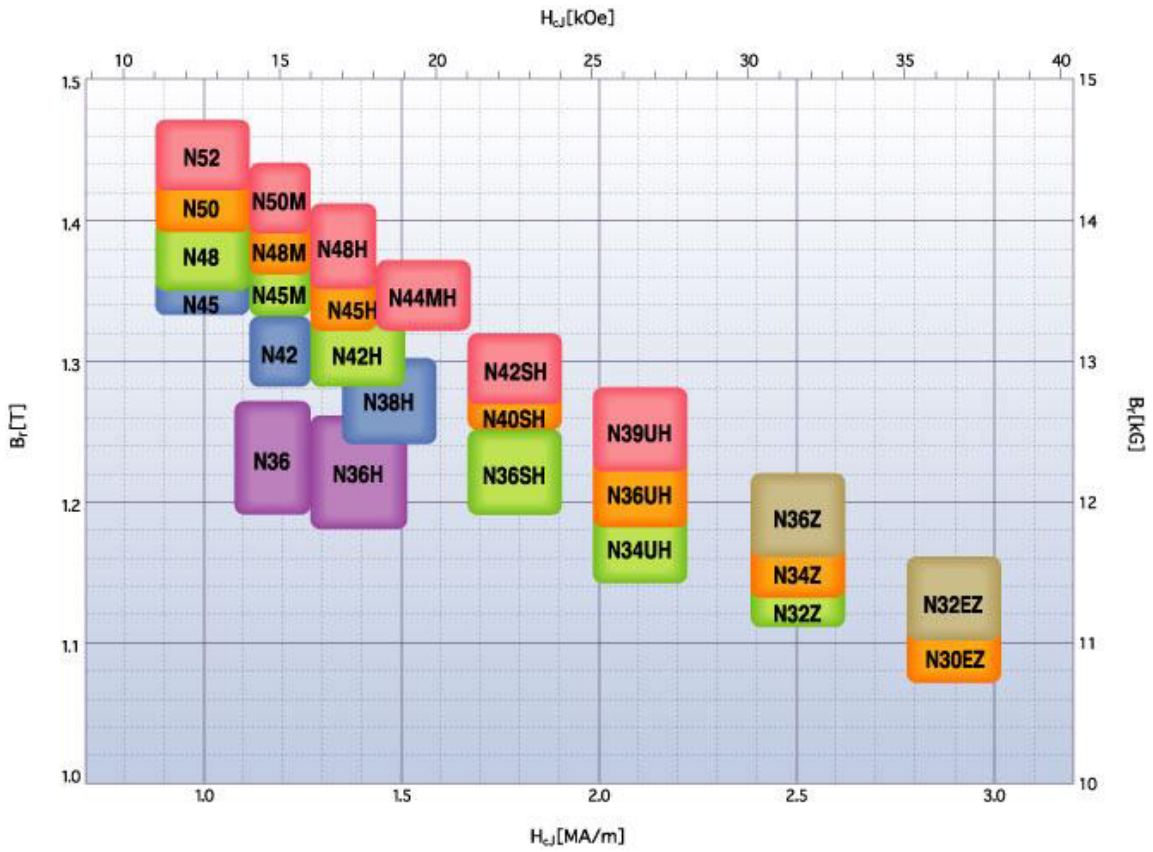

Figure 17. Various grades of NdFeB. [120]

The grade of NdFeB used to construct the magnets was 48M. This grade is one of the highest performance NdFeB available (Figure 17). N48M has the following characteristics:

Relative permeability (Mu)	1.45
Conductivity	6.2 S/m
Coercitivity (Hc)	14000 kA/m
Remanence (Br)	1.36-1.41 T
Maximum Energy Product (BH)max	358-390-kJ/m^3

Table 9. Properties of N48M.

These characteristics were used later in the electromagnetic finite element analysis.

[120] Shin-Etsu Magnetics Inc.

http://www.shinetsumagnetics.com/n_series_magnetic_performance_di.htm

4.2 Characterization of Field and Gradient

A THM 7025 3-Axis Hall Teslameter was used to accurately measure and spatially map the field and gradient of the system. Three Hall elements are used in this device to measure the different components of the B field. The elements that measure B_x, B_y and B_z are located within a 3mm diameter sphere at the end of the probe. One can assume that the center of this sphere is approximately the center of the active sensor volume with a range of 0.01 mT- 2 T (Figure 18).

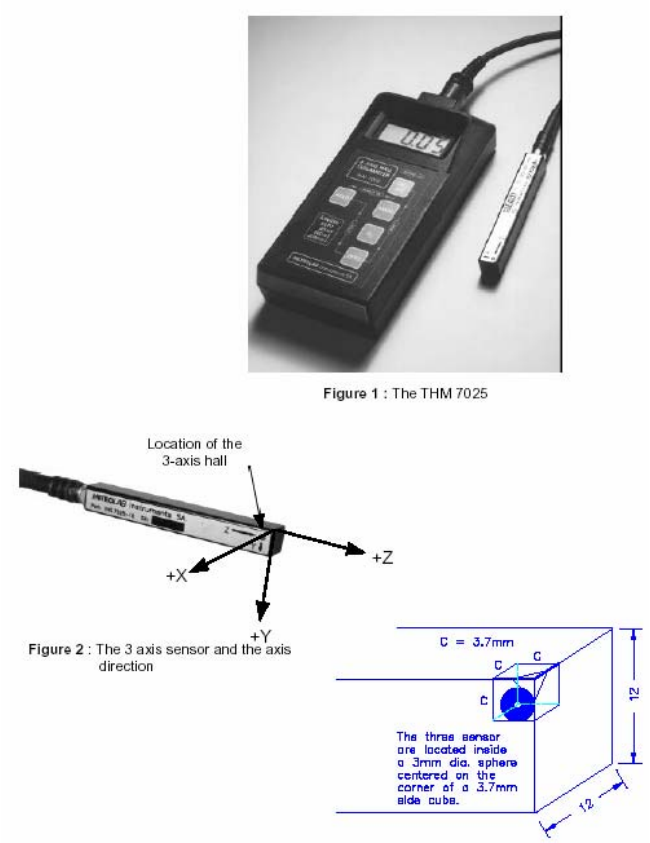

Figure 18. The THM 7025 3-Axis Hall Teslameter[121]

[121] MetroLab THM 7025 Users Manual. Version 2.01. Revision 1.4. September 1997.

Magnetic simulations were performed to predict the fields and gradients with Ansoft's 3D Electromagnetic Finite Element Analysis.

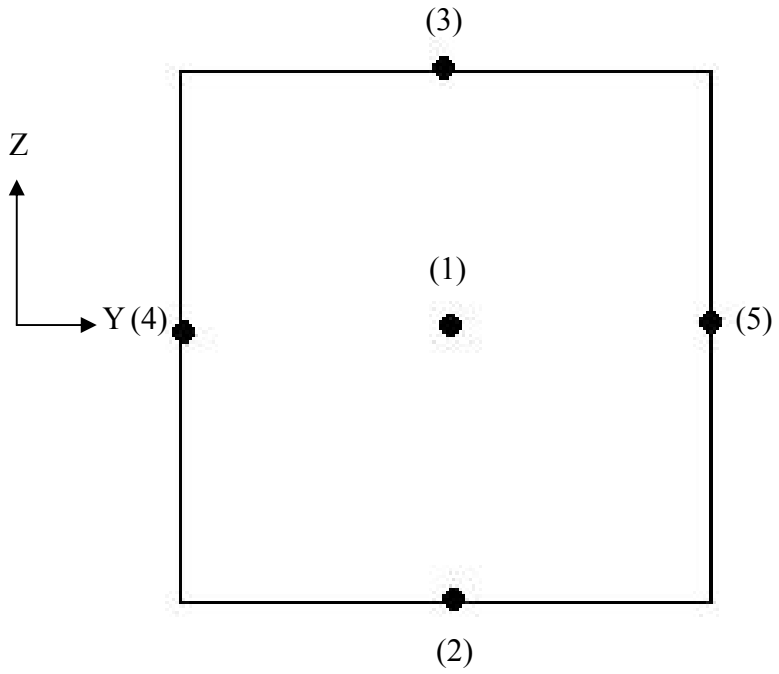

Figure 19. Side view of the right field magnet and the corresponding traces made in Z-Y plane.

The magnetic investigation system was characterized by comparing the predicted theoretical results with experimental field measurements. Measurements on the system shown in Figure 12 were taken starting on the face of the right field magnet, along the x-axis going left every 12 mm with a 1.25-inch separation of each field magnet from the center gradient magnet. Five different traces were completed in this fashion in the Z-Y plane (Figure 19). The total B field predicted in Figure 20 compared with the total B field measured is shown to agree as noted by the total B field ranging from 0.5T near the face of the right field magnet, dropping to 0.3 T near the center gradient magnet, and 0.5T near the left field magnet.

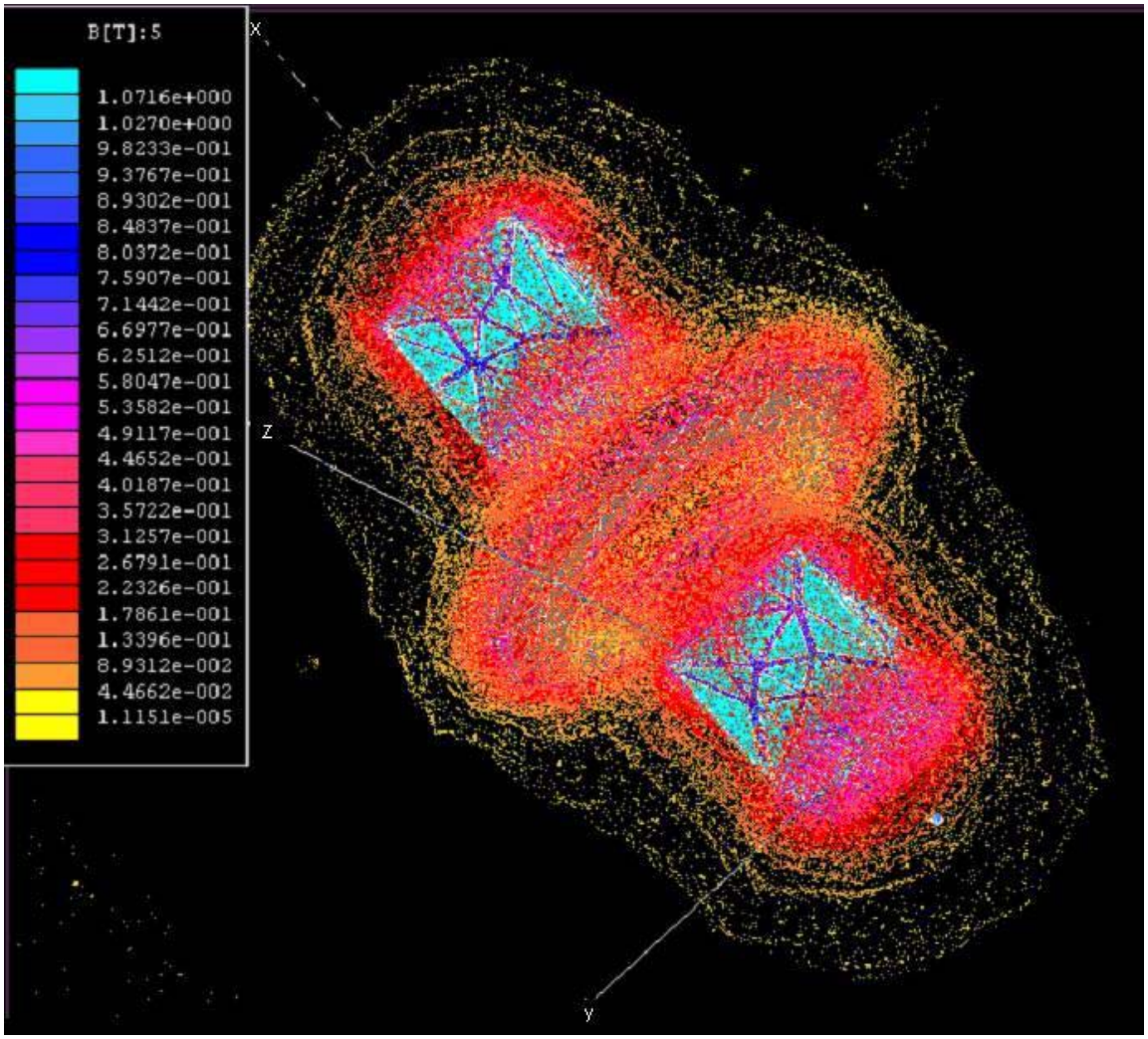

TOTAL MEASURED B FIELD				
CENTERLINE (1)	**BOTTOM (2)**	**TOP (3)**	**FAR (4)**	**NEAR (5)**
0.548	0.48	0.571	0.514	0.546
0.464	0.356	0.418	0.371	0.523
0.368	0.298	0.267	0.263	0.284
0.314	0.272	0.186	0.196	0.118
0.387	0.315	0.342	0.378	0.324
0.44	0.372	0.45	0.444	0.4
0.587	0.565	0.669	0.635	0.534

Figure 20. Theoretical field strengths predicted using ANSOFT's 3D Maxwell Equation Finite Element Analysis Software compared to measured values.

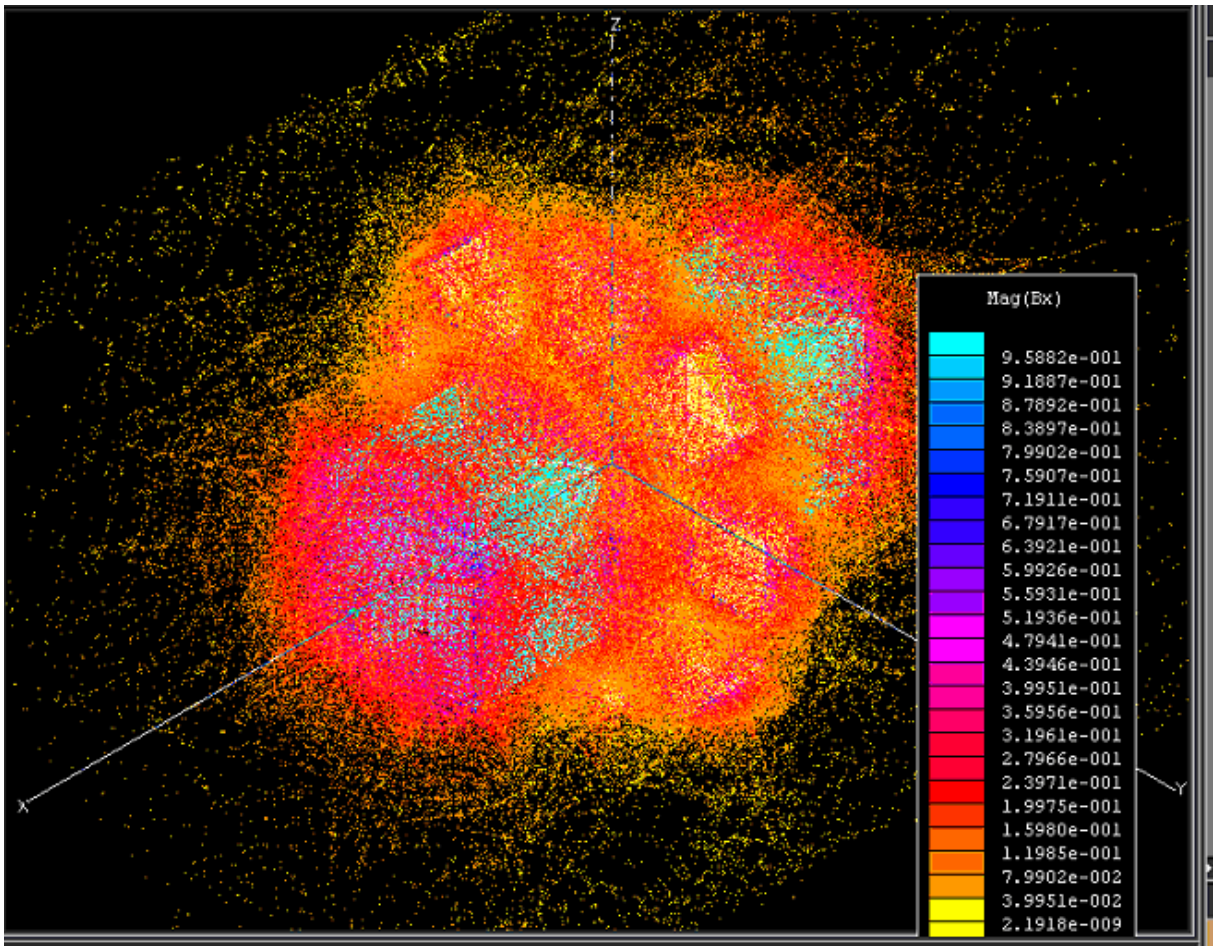

TOTAL X -COMPONENT OF B FIELD				
CENTERLINE (1)	**BOTTOM (2)**	**TOP (3)**	**FAR (4)**	**NEAR (5)**
-0.55	-0.252	-0.478	-0.417	-0.421
-0.481	-0.268	-0.365	-0.324	-0.252
-0.376	-0.227	-0.264	-0.312	-0.27
-0.292	-0.1609	-0.197	-0.1609	-0.1094
-0.407	-0.271	-0.24	-0.312	-0.261
-0.462	-0.262	-0.257	-0.36	-0.277
-0.594	-0.496	-0.508	-0.433	-0.445

Figure 21. Total X-Component of B Field.

The total x-component of the B field predicted in Figure 21 compared with the total x-component of the B field measured is shown to agree as noted by the B field ranging from 0.5T near the face of the right field magnet, dropping to 0.3 T near the center gradient magnet, and 0.5T near the left field magnet.

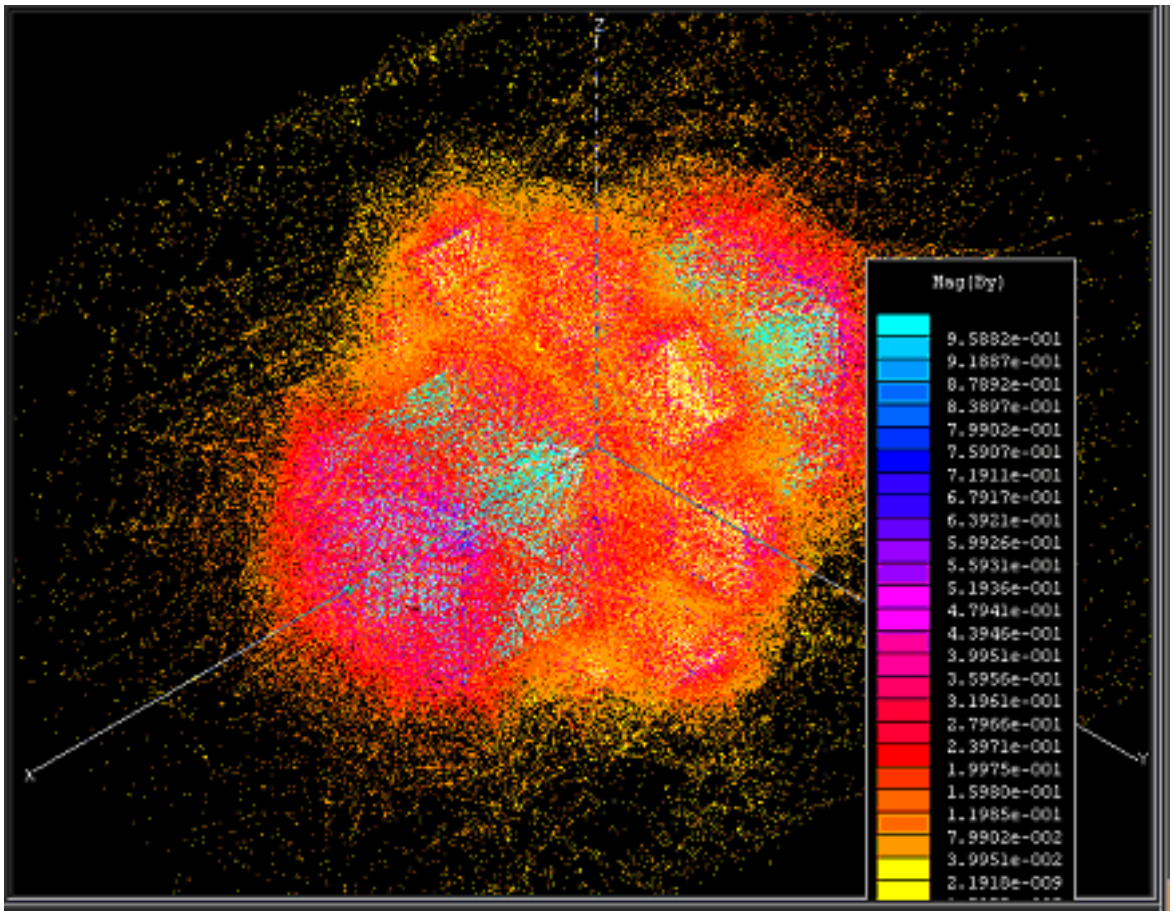

TOTAL Y-COMPONENT OF B FIELD				
CENTERLINE (1)	**BOTTOM (2)**	**TOP (3)**	**FAR (4)**	**NEAR (5)**
-0.0025	-0.00472	0.00917	0.409	-0.484
-0.032	0.01358	0.004	0.296	-0.29
-0.0453	0.041	0.00005	0.1236	-0.195
-0.051	0.01647	-0.00417	0.0653	-0.114
-0.0119	0.0034	0.00601	-0.1053	0.1427
0.0286	0.0266	-0.00829	-0.169	0.1619
-0.004	-0.032	-0.0099	-0.353	0.227

Figure 22. Total Y-Component of B Field.

The total y-component of the B field predicted in Figure 22 compared with the total y-component of the B field measured agrees closely (especially within the centerline). It is most important to note that the x-component along the centerline is clearly dominant by comparison with Figure 21.

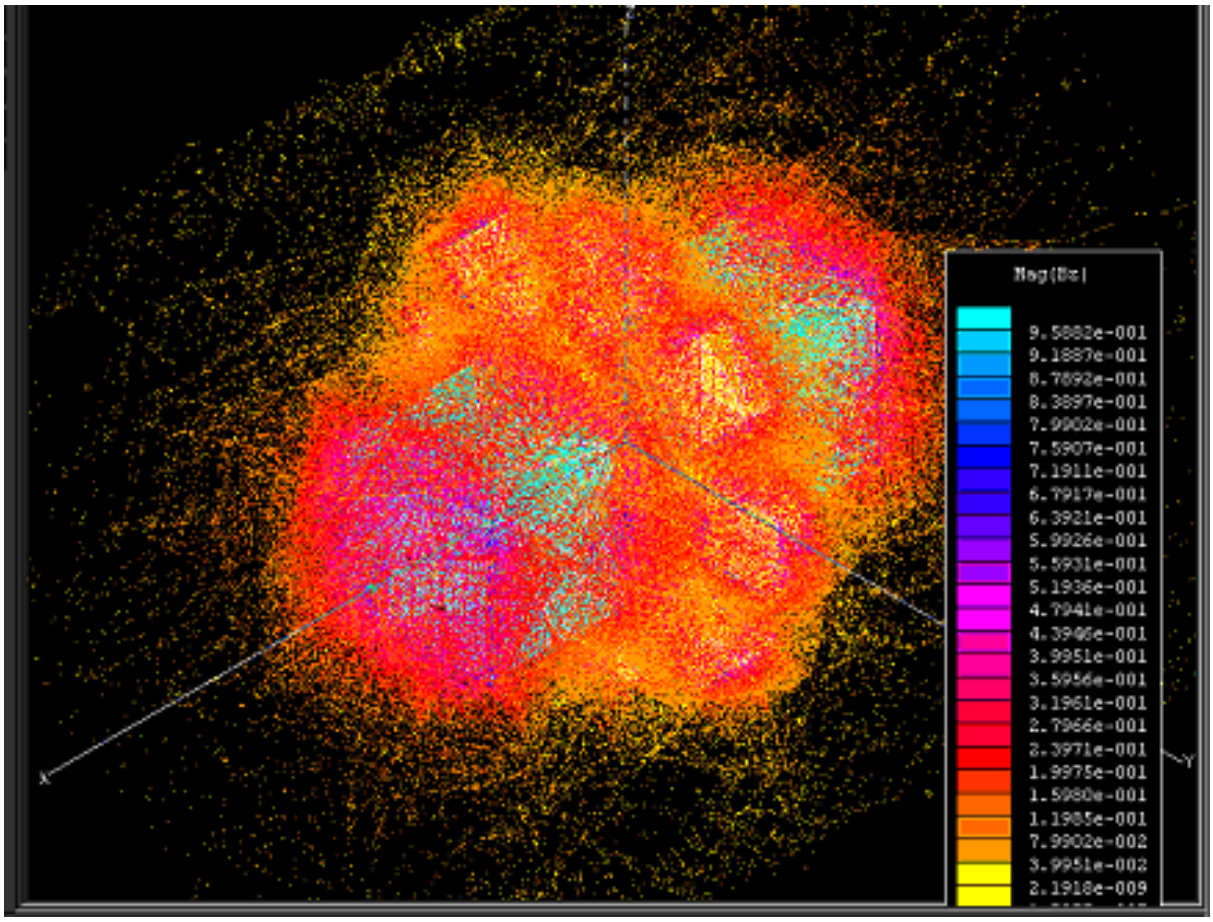

TOTAL Z-COMPONENT OF B FIELD				
CENTERLINE (1)	**BOTTOM (2)**	**TOP (3)**	**FAR (4)**	**NEAR (5)**
0.0197	0.312	-0.327	0.00887	0.0341
0.0238	0.202	-0.236	-0.01535	0.0279
-0.01414	0.1086	-0.1276	-0.00563	0.00136
0.0262	0.0146	0.0213	-0.00411	-0.0007
0.0568	-0.156	0.254	0.0059	0.00863
0.0641	-0.271	0.339	0.00038	-0.0258
0.0524	-0.367	0.404	0.0323	0.01731

Figure 23. Total Z-Component of B Field.

The total z-component of the B field predicted in Figure 23 compared with the total z-component of the B field measured is shown to agree closely (especially within the centerline). It is most important to note again that the x-component along the centerline is clearly dominant by comparison with Figure 21.

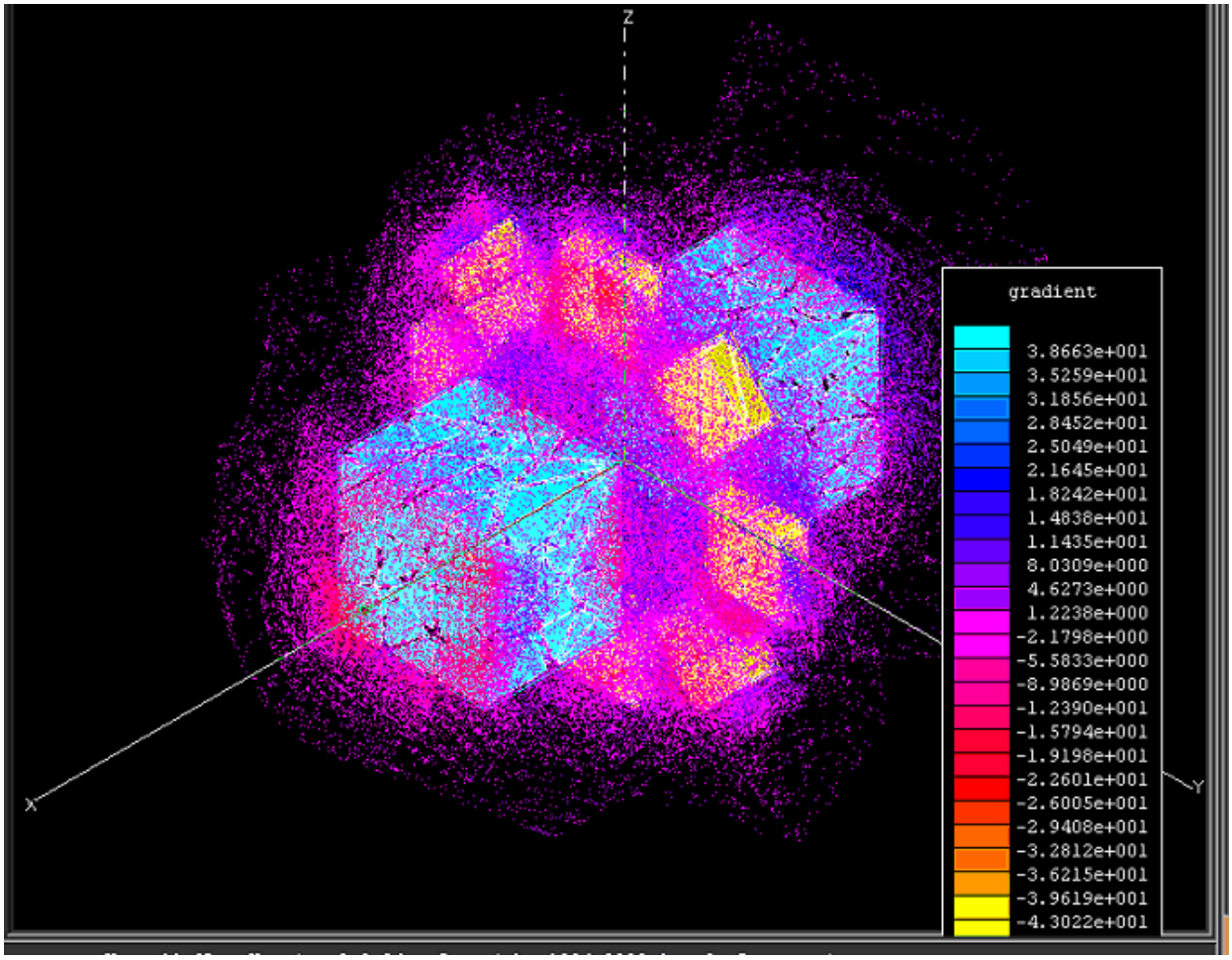

TOTAL X-COMPONENT GRADIENT OF B FIELD				
CENTERLINE (1)	**BOTTOM (2)**	**TOP (3)**	**FAR (4)**	**NEAR (5)**
-5.7500	1.3333	-9.4167	-7.7500	-14.0833
-8.7500	-3.4167	-8.4167	-1.0000	1.5000
-7.0000	-5.5083	-5.5833	-12.5917	-13.3833
9.5833	9.1750	3.5833	12.5917	12.6333
4.5833	-0.7500	1.4167	4.0000	1.3333
11.0000	19.5000	20.9167	6.0833	14.0000

Figure 24. Total X-Component Gradient of B Field.

The total x-component gradient of the B field predicted in Figure 24 compared with the total x-component of the B field measured is shown to agree closely (especially along the centerline).

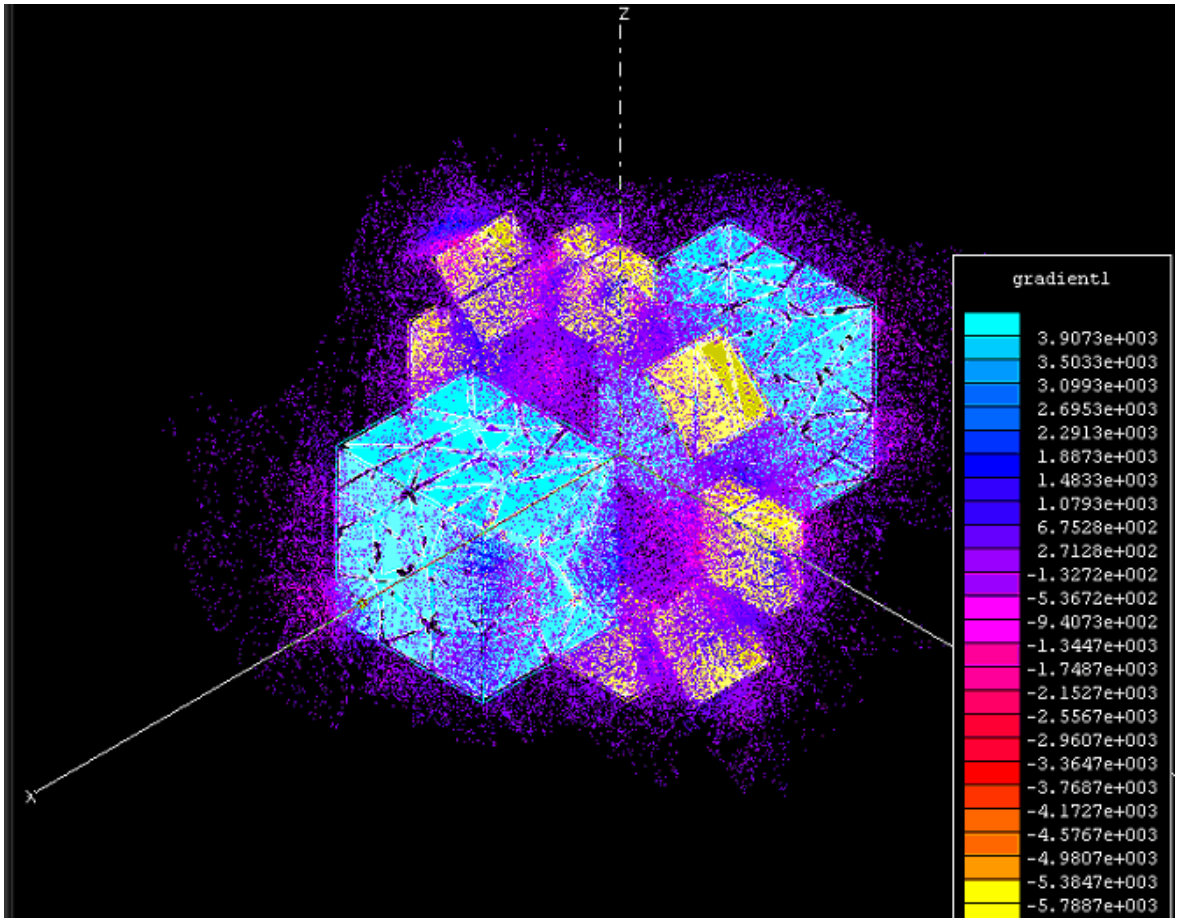

TOTAL Y-COMPONENT GRADIENT OF B FIELD				
CENTERLINE (1)	**BOTTOM (2)**	**TOP (3)**	**FAR (4)**	**NEAR (5)**
2.4583	-1.5250	0.4308	9.4167	-16.1667
1.1083	-2.2850	0.3292	14.3667	-7.9167
0.4750	2.0442	0.3517	4.8583	-6.7500
-3.2583	1.0892	-0.8483	14.2167	-21.3917
-3.3750	-1.9333	1.1917	5.3083	-1.6000
2.7167	4.8833	0.1342	15.3333	-5.4250

Figure 25. Total Y-Component Gradient of B Field.

The total y-component gradient of the B field predicted in Figure 25 compared with the total z-component of the B field measured agree closely (especially within the centerline). It is most important to note again that the y-component along the centerline is dominant by comparison with Figure 24 and the higher variance shown in the values of Figure 25.

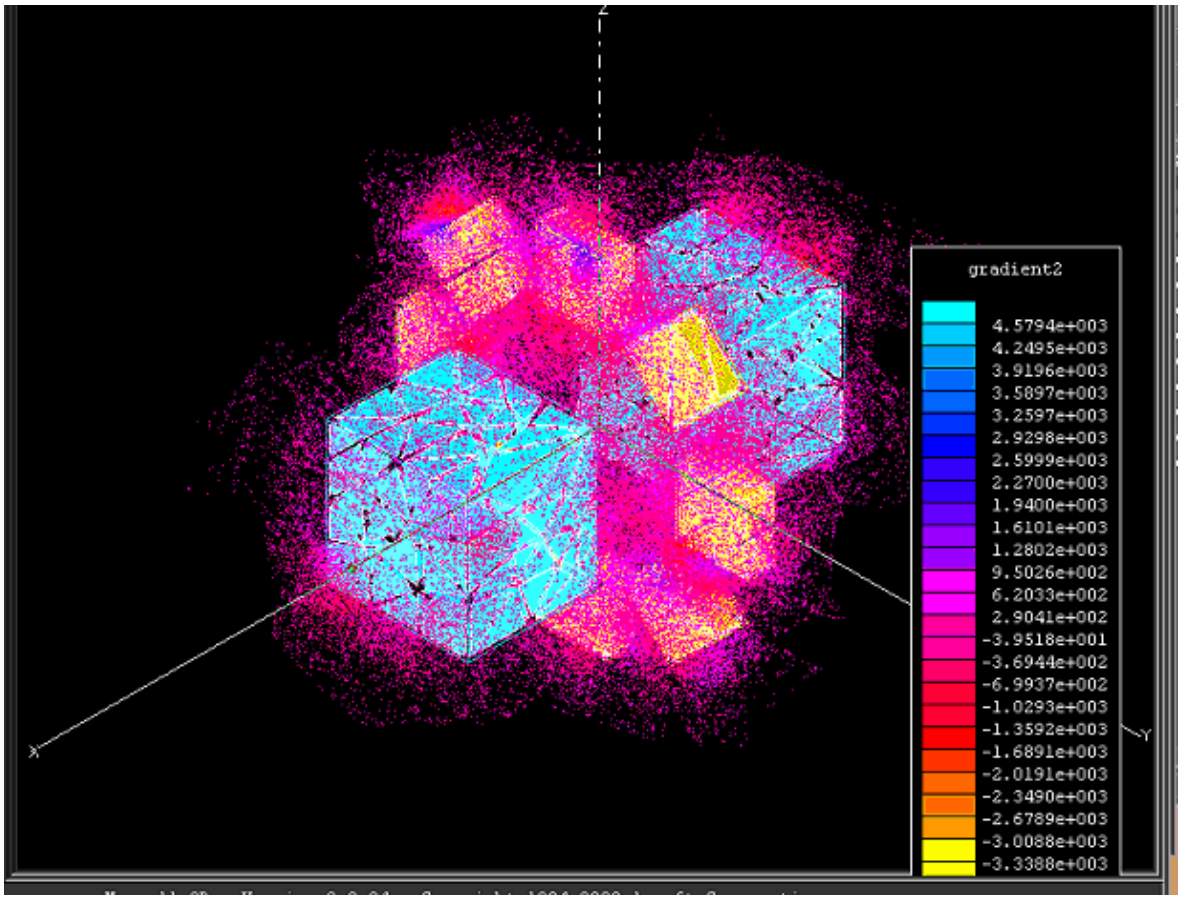

TOTAL Z-COMPONENT GRADIENT OF B FIELD				
CENTERLINE (1)	**BOTTOM (2)**	**TOP (3)**	**FAR (4)**	**NEAR (5)**
-0.3417	9.1667	-7.5833	2.0183	0.5167
3.1617	7.7833	-9.0333	-0.8100	2.2117
-3.3617	7.8333	-12.4083	-0.1267	0.1717
-2.5500	14.2167	-19.3917	-0.8342	-0.7775
-0.6083	9.5833	-7.0833	0.4600	2.8692
0.9750	8.0000	-5.4167	-2.6600	-3.5925

Figure 26. Total Z-Component Gradient of B Field.

The total z-component gradient of the B field predicted in Figure 26 compared with the total z-component of the B field measured tend to agree (especially within the centerline). It is most important to note again that the z-component along the centerline is dominant by comparison with Figure 24 and the higher variance shown in the values of Figure 25.

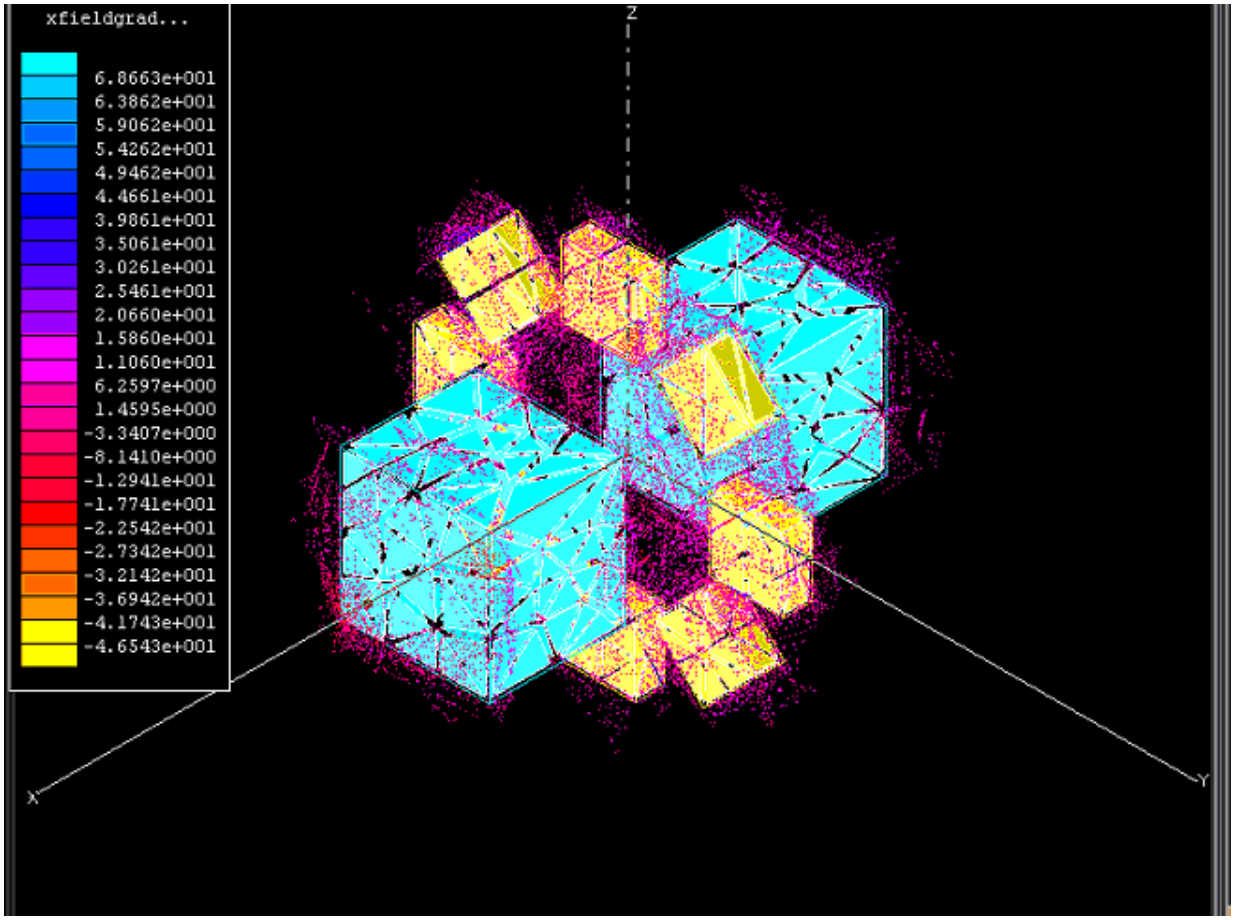

TOTAL X-COMPONENT GRADIENT OF B FIELD * X-COMPONENT OF B FIELD				
CENTERLINE (1)	**BOTTOM (2)**	**TOP (3)**	**FAR (4)**	**NEAR (5)**
3.1625	-0.3360	4.5012	3.2318	5.9291
4.2088	0.9157	3.0721	0.3240	-0.3780
2.6320	1.2504	1.4740	3.9286	3.6135
-2.7983	-1.4763	-0.7059	-2.0260	-1.3821
-1.8654	0.2033	-0.3400	-1.2480	-0.3480
-5.0820	-5.1090	-5.3756	-2.1900	-3.8780

Figure 27. Total X-Component Gradient of B Field * X-Component of B Field.

The total product of the x-component gradient and the x-component of the B field predicted in Figure 27 compared with the product of the x-component gradient and the x-component of the B field measured is shown to agree as noted by values ranging close to one within the predicted and experimental values.

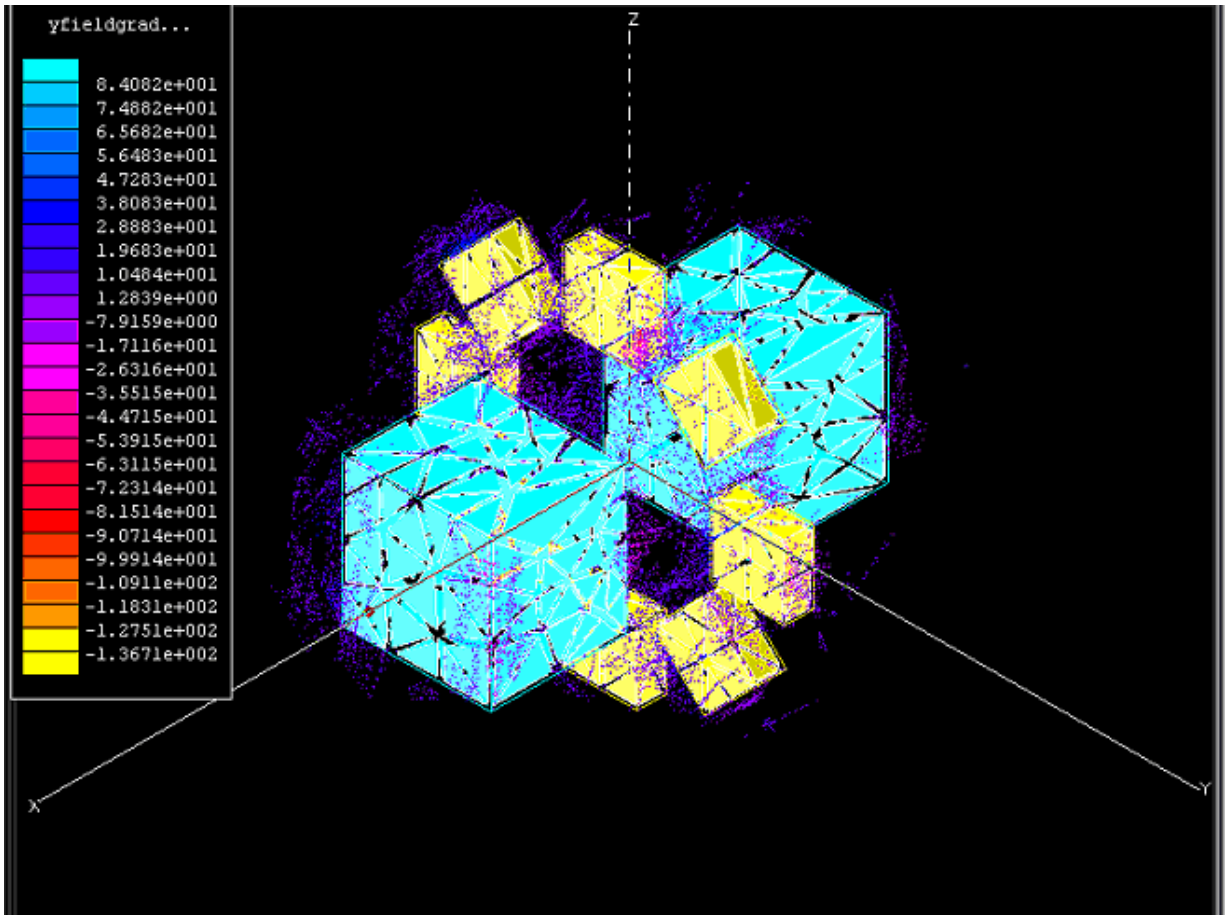

TOTAL Y-COMPONENT GRADIENT OF B FIELD * Y-COMPONENT OF B FIELD				
CENTERLINE (1)	**BOTTOM (2)**	**TOP (3)**	**FAR (4)**	**NEAR (5)**
-0.0061	0.0072	0.0040	3.8514	7.8247
-0.0355	-0.0310	0.0013	4.2525	2.2958
-0.0215	0.0838	0.0000	0.6005	1.3163
0.1662	0.0179	0.0035	0.9283	2.4387
0.0402	-0.0066	0.0072	-0.5590	-0.2283
0.0777	0.1299	-0.0011	-2.5913	-0.8783

Figure 28. Total Y-Component Gradient of B Field * Y-Component of B Field.

The total product of the y-component gradient and the y-component of the B field predicted in Figure 28 compared with the product of the y-component gradient and the y-component measured it is important to note the lower magnitude and higher variance to that of the total product of the x-component gradient and the x-component of the B field.

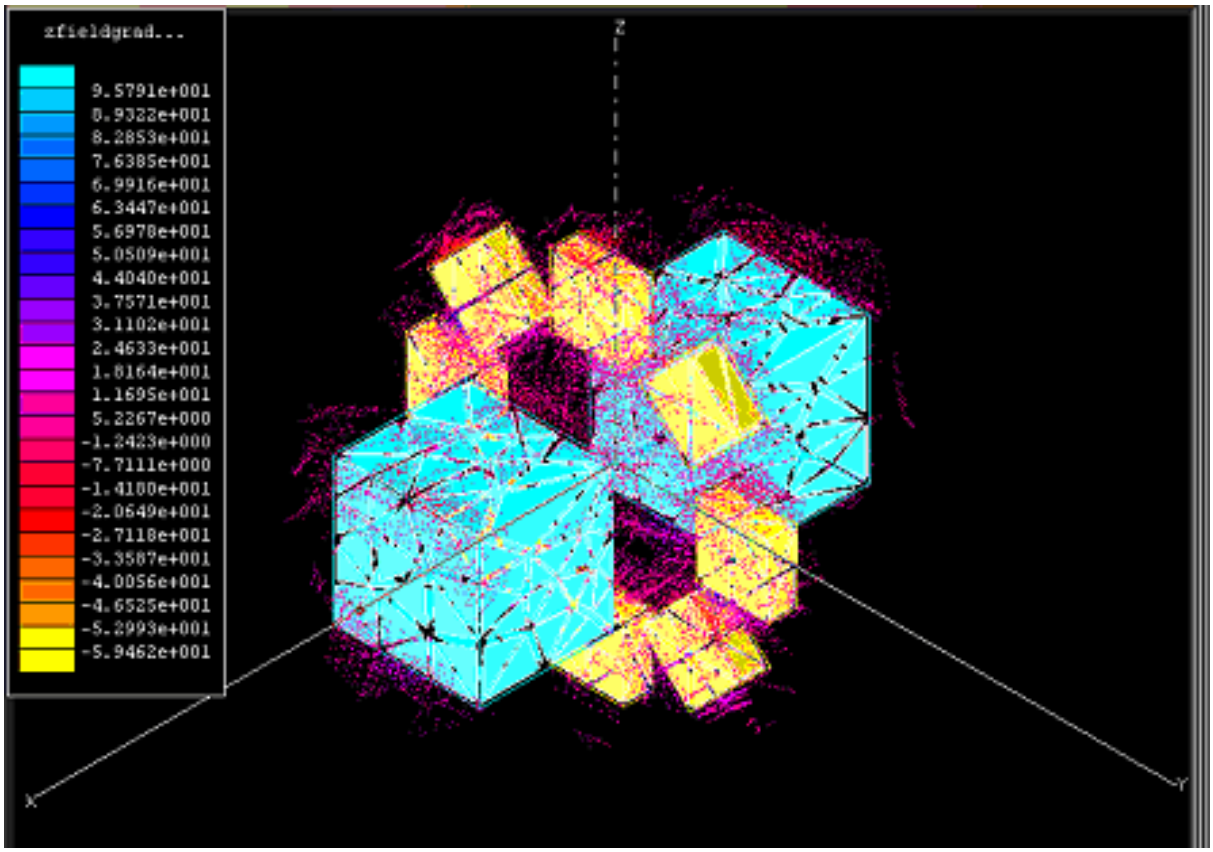

TOTAL Z-COMPONENT GRADIENT OF B FIELD * Z-COMPONENT OF B FIELD				
CENTERLINE (1)	**BOTTOM (2)**	**TOP (3)**	**FAR (4)**	**NEAR (5)**
-0.0067	2.8600	2.4798	0.0179	0.0176
0.0752	1.5722	2.1319	0.0124	0.0617
0.0475	0.8507	1.5833	0.0007	0.0002
-0.0668	0.2076	-0.4130	0.0034	0.0005
-0.0346	-1.4950	-1.7992	0.0027	0.0248
0.0625	-2.1680	-1.8363	-0.0010	0.0927

Figure 29. Total Z-Component Gradient of B Field * Z-Component of B Field.

The total product of the z-component gradient and the z-component of the B field predicted in Figure 29 compared with the product of the z-component gradient and the z-component measured it is important to note the lower magnitude and higher variance to that of the total product of the x-component gradient and the x-component of the B field.

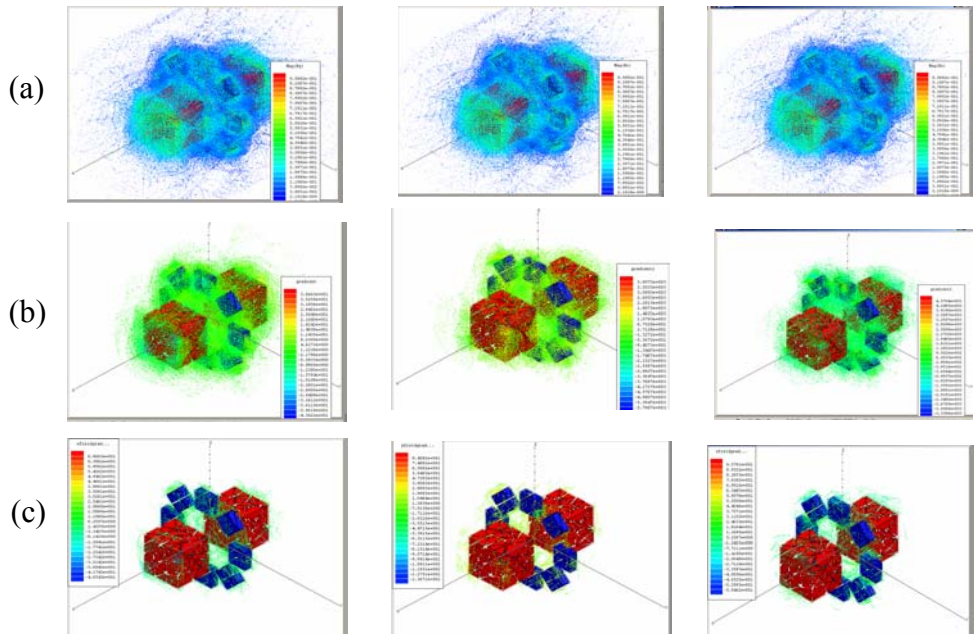

Figure 30. Composite View. From left to right: (a)Magnitude of Field in the x-plane, y-plane, and z-plane. (b) Gradient in the x-plane, y-plane, and z-plane. (c) Field-Gradient product in the x-plane, y-plane and z-plane.

The constituent analysis of the field and gradient in every direction and volume was performed to characterize the workspace between the magnets. Since the field and gradient varied over the entire workspace volume, we needed to find the volume elements with the highest field and gradient with the smallest amount of variation in a given volume. The chosen experimental volume of 0.64 cm^3 meeting these criteria is located on the right face of the center gradient magnet (offset from the geometric center of the circular gradient magnet).

4.3 Characterization of Magnetic Microspheres

Magnetic properties of microspheres containing magnetite nanoparticles were characterized via vibrating sample magnetometry (Figure 31). The vibrating sample magnetometer operates on the principle that when a sample material is placed in a

uniform magnetic field, a dipole moment proportional to the product of the sample susceptibility times the applied field is induced in the sample. A sample also undergoing sinusoidal motion induces an electrical signal in a set of stationary pick-up coils. This signal is proportional to the magnetic moment, vibration amplitude, and vibration frequency.

Figure 31. The LakeShore 7300 Vibrating Sample Magnetometer.

The material under study is contained in a sample holder, which is centered in the region between the pole pieces of an electromagnet. A vertical sample rod connects the sample holder with a transducer assembly located above the magnet, which supports the transducer assembly with sturdy, adjustable support rods. The transducer then converts a sinusoidal AC drive signal, provided by a circuit located in the console, into a sinusoidal vertical vibration of the sample rod, and the sample thus undergoes a sinusoidal motion in a uniform magnetic field. Coils mounted on the pole pieces of the magnet pick up the signal resulting from the sample motion. This AC signal at the vibration frequency is proportional to the magnitude of the moment induced in the sample, vibration amplitude and frequency. A servo system maintains constancy in the drive amplitude and frequency so that the output accurately tracks the moment level without degradation due to variations in the amplitude and frequency of vibration. The complete system operation is summarized in Figure 32.

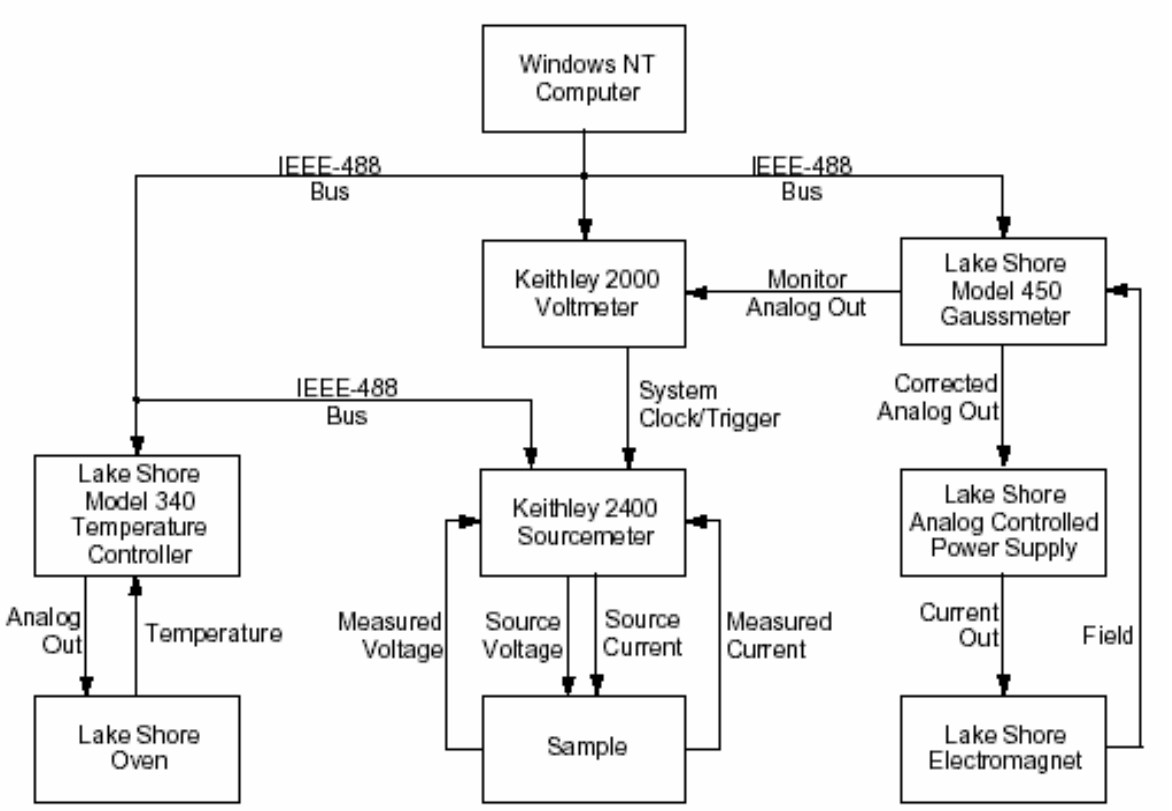

Figure 32. Flowchart of VSM operations.[122]

The samples can be characterized by weight or volume. Dry microsphere samples were weighed and fluids were injected into the sample holder (0.05 mL). The VSM was ramped to full field and the highest sensitivity allowed for the selected material. The field was ramped from 0.8 T to –0.8T and back to 0.8 T over a period of 30 minutes. An exemplary magnetic response for Dynabeads Product 142.04 (Table 10), is provided in Figure 33. This material was in the form of uniform, superparamagnetic, polystyrene beads coated with a polyurethane layer. The data confirmed that these microspheres did not exhibit hysteresis as in (Figure 34).

[122] User's Manual. Lakeshore 7300 Series. VSM System. February 2001.

Physical characteristics	
Diameter	2.8 μm ± 0.2 μm (C.V. max 5%)
Surface area	4-8 m^2/g
Active chemical functionality	50-70 μmol/g Dynabeads
Density	1.3 g/cm^3
Iron content	approx. 12%
Magnetic mass susceptibility	100 ± 25 x 10^{-6} m^3/kg
Concentration	2 x 10^9 beads/ml (approx. 30 mg/ml)

Table 10. Physical Characteristics of Dynabeads M-280 Magnetic Microspheres.[123]

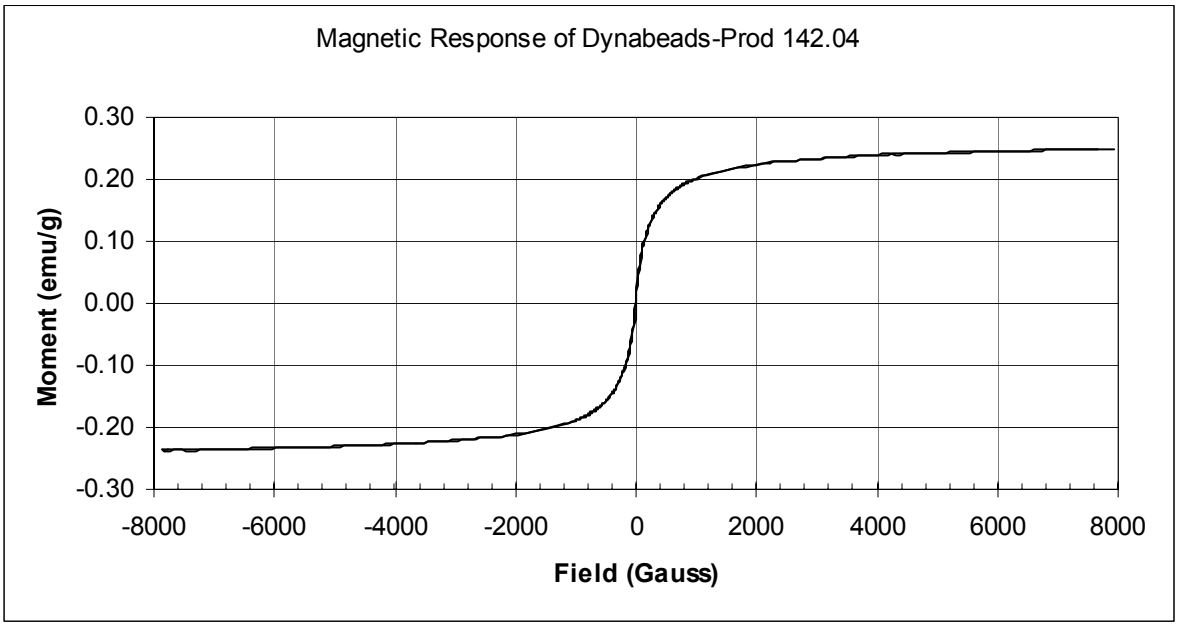

Figure 33. VSM Characterization of Dynabeads Product Number 142.04.

[123] Product Literature for Dynal Biotech Product Number 142.04. 2001.

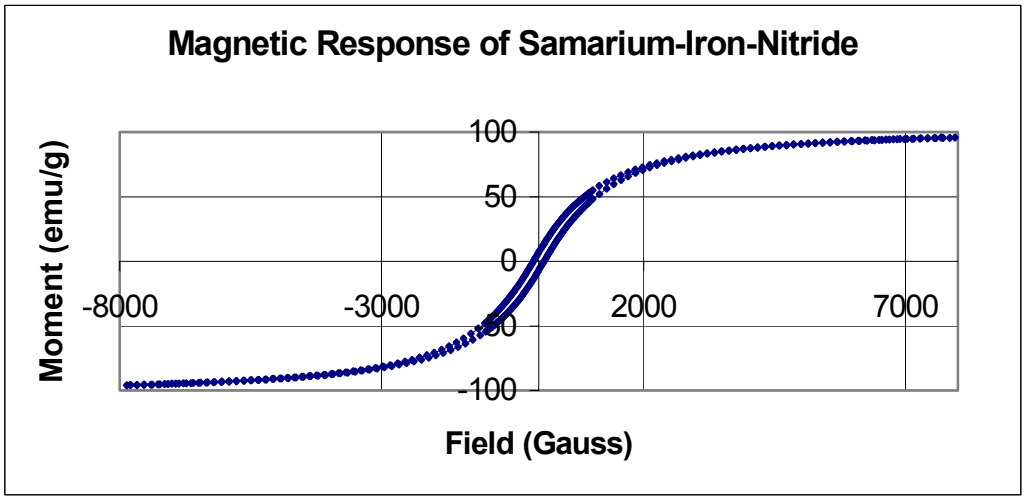

Figure 34. VSM Characterization of Multi-Domain Samarium-Iron-Nitride.

4.4 Characterization of Microspheres Under Flow Conditions

4.41 Electromagnet-Induced Magnetic Particle Motion

Initial investigations of a ferrofluid were conducted by placing powered Manganese Zinc (MnZn) in a closed tube (under zero flow), filling the tube with water and demonstrating magnetic guidance in one dimension along the tube. The MnZn particles were 281 microns in diameter (± 10 microns). They had a specific magnetic saturation of 80 emu/g, a concentration of approximately 1.14 g/cm^3. The force experienced by a single MnZn particle near the coil was approximately 1.33 x 10^{-8} N. In the Faraday Lab of Virginia Tech the tube was arranged between two electromagnet coils oriented so the magnetic vector fields of the two coils were anti-parallel along the long axis of the tubes (Figure 35). Starting with zero electrical currents applied to both coils, the current supplied to one coil was increased (to obtain approximately 1 T at the coil) until the MnZn in the dispersion moved to one end of the tube. The current supplied to the first coil was then decreased to zero and the current supplied to the other coil increased until the MnZn moved to the opposite end of the tube. It should be noted that the MnZn particles were large compared to the micrometer size of the magnetite microspheres and

thus the MnZn particles had a high response. This demonstrated guidance in one dimension.

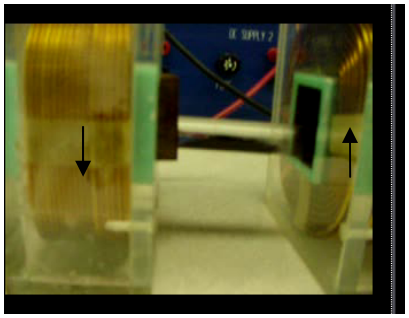

Figure 35. Manipulation of a ferrofluid with electromagnets (Arrows depict current direction).

4.42 Fixed Magnet Microsphere Control

Additional experiments were conducted at Stereotaxis, Inc. in St. Louis, Missouri to probe the dynamics of magnetically guiding magnetic microspheres. Dynabead's magnetic microsphere Product 142.04, consisting of a density of 1.3 g/cm^3, iron content of 12%, a concentration of 2 x 10^9 beads/ml, was obtained from Dynal Biotech. A volume of 0.5 mL was injected into a small test cell and threaded into a load cell by a 10/32" nonmagnetic plastic screw. The test magnet system was set at the highest gradient, 0.9 Tesla/m, and field strength, 0.09 Tesla, allowed by the system. These values were confirmed with a 3-axis #7025 Metrolab Hall Teslameter. The dynabeads exterted a force of 0.0075 N on the load cell in the configuration shown in Figure 36. The ferrofluid was confined to one side of the holder by the magnetic field and gradient, overcoming gravitational, surface tension and other forces (Figure 37). This experiment demonstrated an effective method of measuring the force a ferrofluid produces in a given magnetic field and gradient.

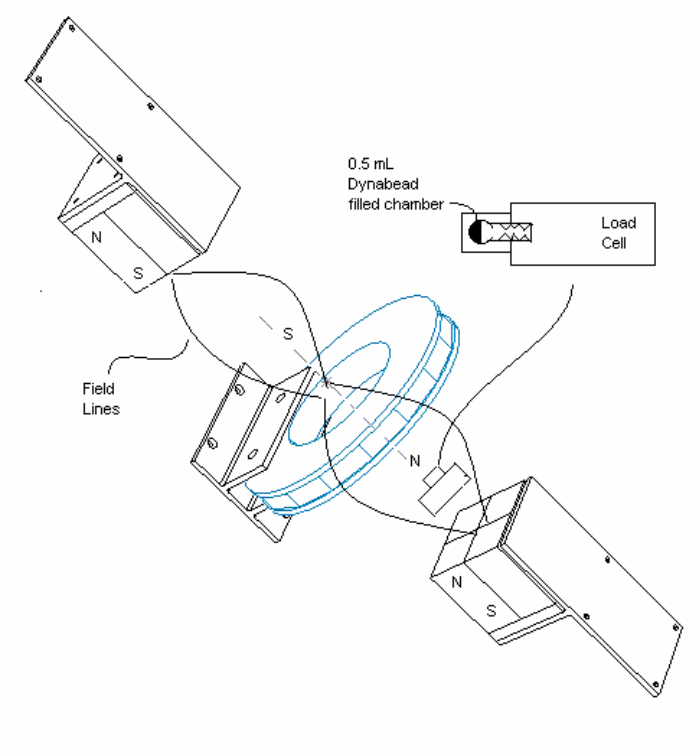

Figure 36. Experimental setup for load testing of microspheres.

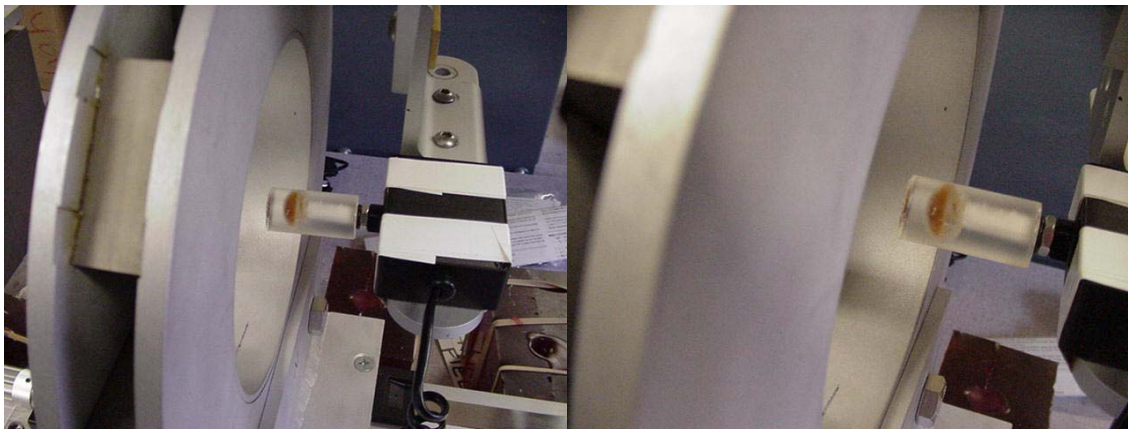

Figure 37. Suspended solution of Dynabeads product 142.04 under static flow conditions.

The effect of fluid flow on the ability to guide magnetic microspheres was also investigated. The fluid flow parameters consisted of a pressure of 120 mmHg (which effects the fluid flow), and a mean velocity of 125 cm/s corresponding to a flow rate of

1.9 liters/minute. A fluid consisting of 5% glycerol and 95% water was used to simulate the viscosity of blood. The fluid flowed through a 0.4 cm (~3/16") inner diameter tube pumped by a Cole-Parmer SY-07554-90 Masterflex L/S Economy Drive Pump with SY-2201-62 Easy-Load Pump Head. This was considered a challenging set of conditions where guidance and control of the magnetic particles was needed.

The 5% glycerol (26 mL), 95% water (500mL), and 0.4mL of the dynabead solution was mixed in a Nalgene bottle to give a brownish dispersion. All fields and gradients were kept identical to the previous experiment while 3/16" inner diameter Nalgene tubing was fed through the center of the magnet (Figure 38). The pump flow was varied from zero flow to the full flow, 125 cm/s. It was observed that the dynabeads remained dispersed in the solution and did not congregate in the magnetic field. This was due to an insufficient magnetic force to counteract the drag force due to a high stream velocity.

Figure 38. Suspended solution of Dynabeads product 142.04 under dynamic flow conditions.

The dynabeads were also injected directly into the tubing within the magnetic field at zero flow (Figure 39). This approach kept the dynabeads from dispersing in the solution. The field and gradient were sufficient to hold the particles in place with relatively no flow. However, there was not sufficient strength to hold the ferro-fluid in place at 1/10 the fluid flow, 12.5 cm/s, that would be experienced in the main arteries. This however does suggest that guidance is possible in a static or low velocity system where the blood flow is temporarily reduced.

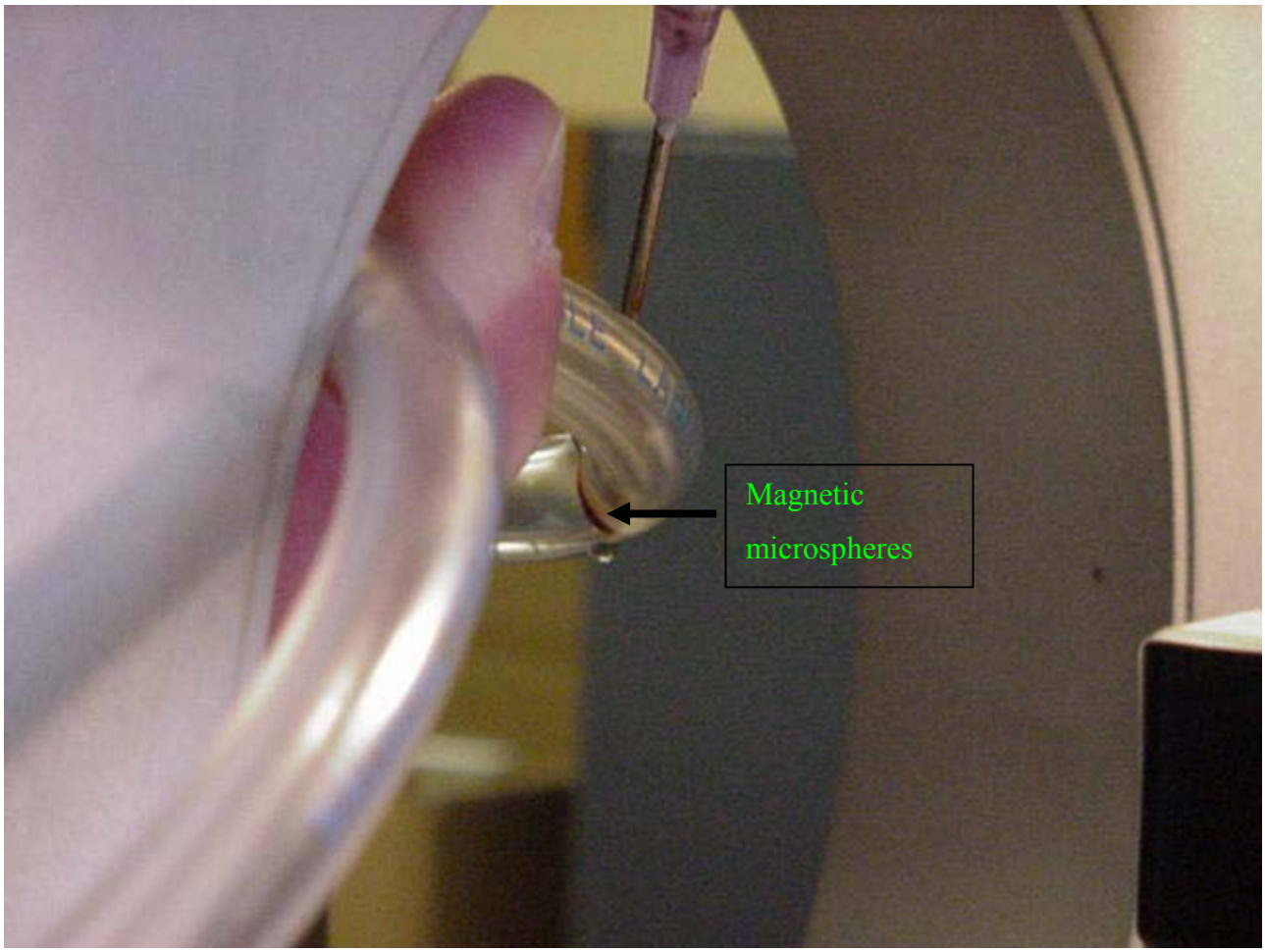

Figure 39. Suspended solution of Dynabead's product 142.04 under variable static/dynamic flow conditions.

4.43 Magnetic Guidance Using Permanent Magnet System at Virginia Tech

Additional experiments with smaller tubing, lower velocities and flow rates, and a higher field-gradient in the new magnetic investigation system were conducted with the objective of confining a group of magnetic microspheres to one side of the tubing during fluid flow (Figure 40). Silicone tubing (Cole Parmer with a 0.64 mm inner diameter) was filled with water using a BD disposable syringe equipped with a Leur-Lok 23 gauge needle.

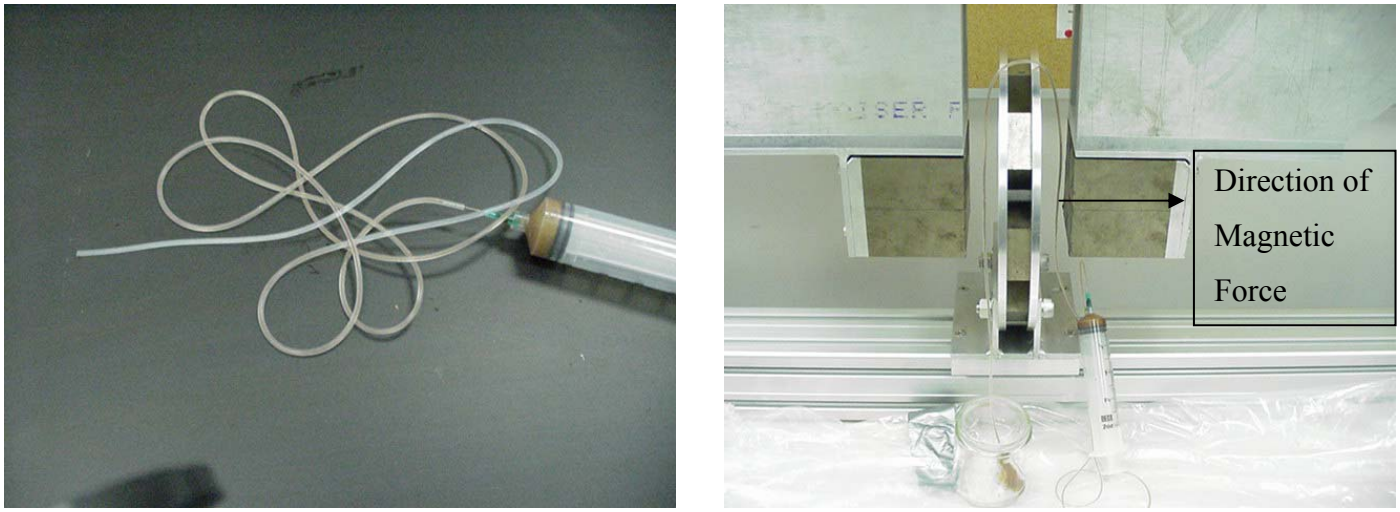

Figure 40. Suspended solution of Dynabead's product 142.04 under dynamic flow conditions with higher field-gradient, smaller tubing size, and slower flow conditions.

Five mL of Dynabead's magnetic microsphere Product 142.04 was injected into the water filled tubing at a rate of approximately 1 ml/min (0.05 cm/s). The tubing was placed in an axial field of 0.3T and a gradient of 13 T/m. The field and gradient component in the other two lines of space was significantly lower compared to the axial direction. Agglomeration of the microspheres or a shift to one side of the tube was not witnessed in this experiment and it appeared that the governing force on microsphere guidance was the fluid flow at 1 ml/min. The magnetic force was expected to be insufficient to hold the Dynabeads stationary in the center of the fluid flow, however it was theorized that frictional forces pushing the Dynabeads against the side of the tubing may allow for agglomeration. Agglomeration of the microspheres may be witnessed with better visualization tools.

Calculations discussed in Section 3.3 indicated that using a 0.3T field and a gradient of 13 T/m, there would be enough magnetic force to manipulate a particle with larger mass at a flow rate of 1 mL/min. An Olympus AX-70 Confocal microscope was used to measure the particle size of a sample of MnZn. Examination of 5 MnZn particles displayed a uniform size of 281 ± 10 microns (Figure 41) and was found to have a magnetic moment of 80 emu/g (Figure 42).

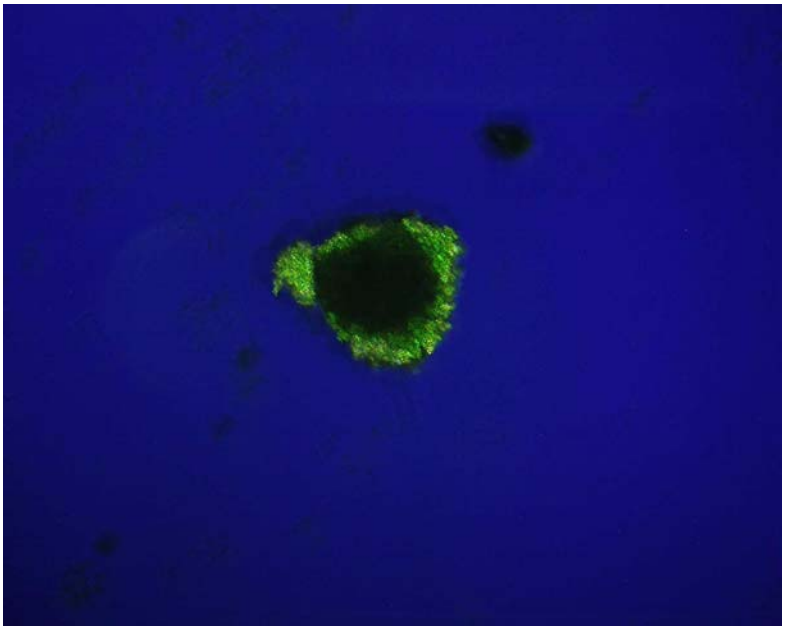

Figure 41. Characteristic 281 micron MnZn sample.

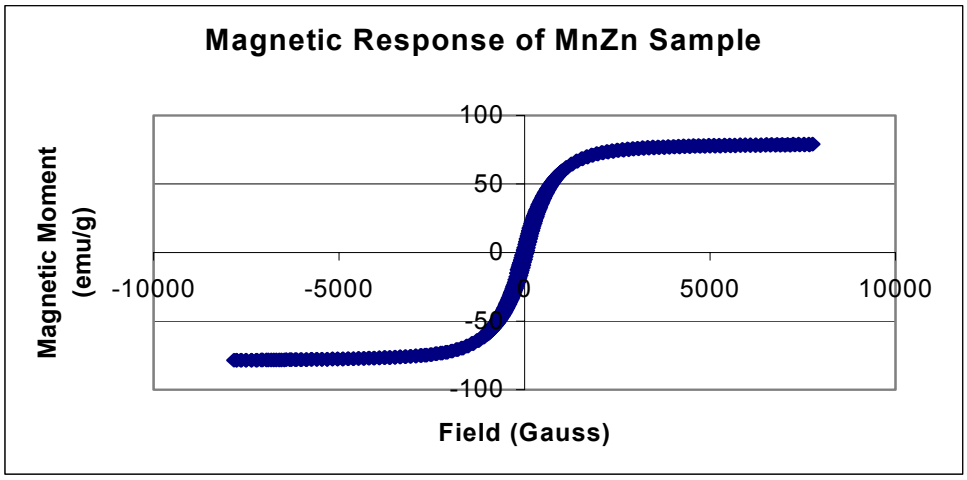

Figure 42. VSM Characterization of MnZn.

This hypothesis held true when tested (Figure 43). 1 cc MnZn powder was mixed with 20 cc of deionized water, and injected through tubing at a rate of 1 mL/min. It was observed that the MnZn was suspended against the side of the tubing while deionized water flowed past.

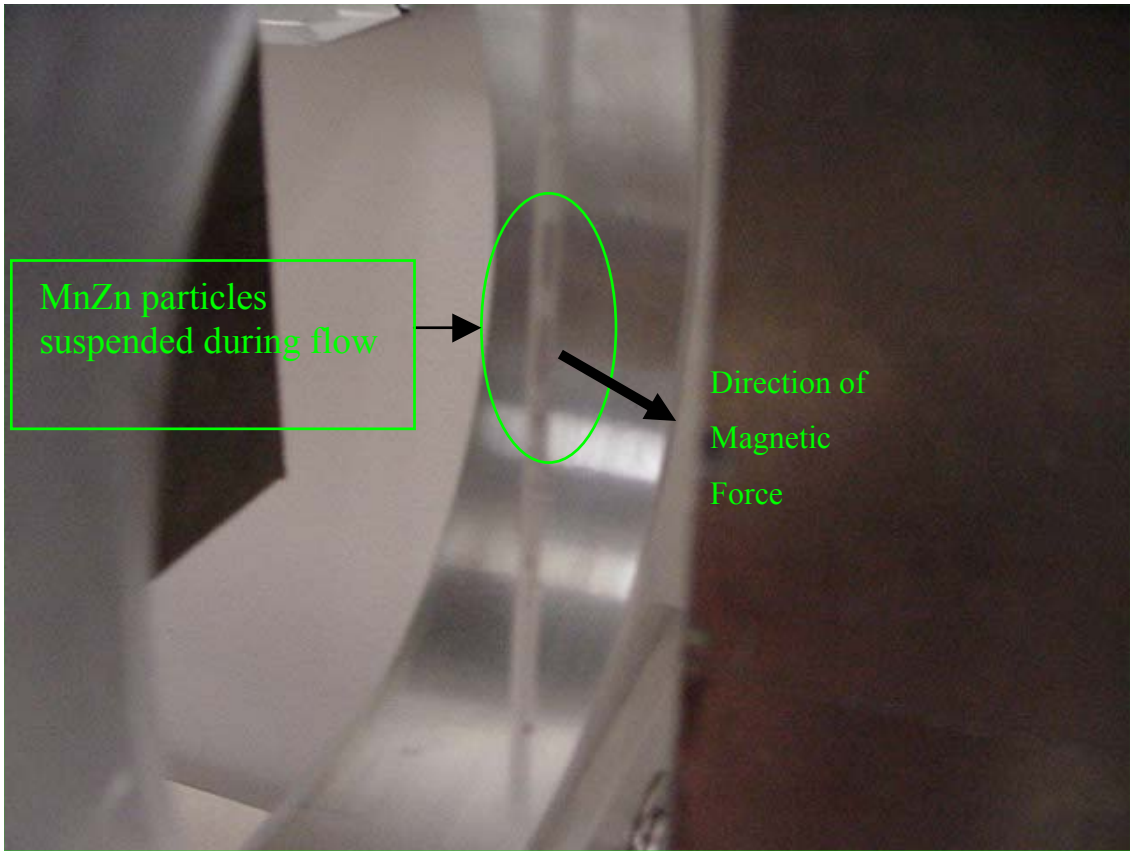

Figure 43. Suspended solution of MnZn under dynamic flow conditions with higher field-gradient, smaller tubing size, and slower flow conditions.

Additional experiments with dynamic field and gradient conditions with flow needed to be conducted to further demonstrate magnetic guidance. In this series of experiments the magnets were moved both away and in parallel to the tubing to vary the magnetic force. Silicone tubing (Cole Parmer with a 0.64 mm inner diameter) was filled with water using a BD disposable syringe equipped with a Leur-Lok 23 gauge needle. 1 cc MnZn powder was mixed with 20 cc of deionized water, and injected through tubing at a rate of 1 mL/min. The tubing was placed in an axial field of 0.3T and a gradient of 13 T/m, parallel to the lab bench. It was again observed that the MnZn was suspended against the side of the tubing while deionized water flowed (Figure 44.a) past since the field and gradient component in the other two lines of space were a couple of degrees of magnitude lower compared to the axial direction as discussed in section 4.2.

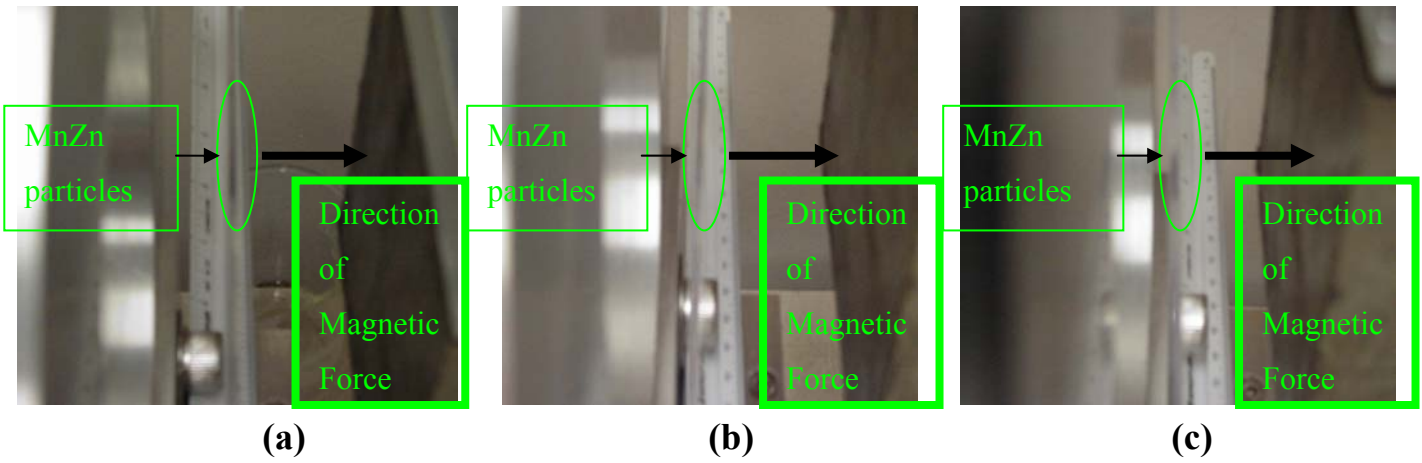

Figure 44. (a.) Suspended solution of MnZn (b.) Outer field magnets moved 1 inch away from the center field magnet, unsuspending particles (c.) Outer field magnets moved 1 inch inward and along direction of tubing to resuspend particles.

The outer field magnets were moved by the system's actuators 1 inch away from the center field magnet. Insufficient magnetic force was then available to localize the MnZn and the drag force carried the particles through the tubing (Figure 44.b). The outer field magnets were then moved 1 inch inward and also along direction of tubing to move the particles to a different location in the tubing (Figure 44.c).

The design and construction of a magnetic particle guidance system was discussed and built. The maximum fields and gradients for this system and thus its overall design were restricted primarily by cost restraints. The restraint for this system that balanced these variables was primarily an active volume of 0.64 cm^3, a workspace clearance of at least an inch on every side, a field of 0.3T, and a local axial gradient of 13 T/m. The 3D electromagnetic finite element analysis modeling matched closely with experimental results. A series of magnetic seeds, were successfully characterized using a vibrating sample magnetometer. Finally, the magnetic seed was investigated under various flow conditions *in vitro* to analyze the effectiveness of the drug delivery system. The effectiveness of the drug delivery system was demonstrated under limiting assumptions

of a specific magnetic field and gradient, seed material, a low fluid flow, and a small volume.

Chapter 5: Conclusion

This thesis reviewed past magnetic drug delivery work, variables, and concepts that needed to be understood for the development of an *in vivo* magnetic drug delivery system. The results of this thesis are the concise study and review of present methods for guided magnetic particles, aggregate theoretical work to allow proper hypotheses and extrapolations to be made, and experimental applications of these hypotheses to a working magnetic guidance system. There have been many uses of magnetic particle manipulation in the human body. However, a single system has yet to emerge that combines those techniques into a simple tool with a wide range of applications extensively used by the medical community.

Specifically the assumptions made in this thesis are the simplification of blood to an average viscosity, a stationary flow force, and low flow rates such as found in the capillaries. Other assumptions that are made are the maximum field and gradient that can be obtained due to cost restraints.

The design and construction of a magnetic particle guidance system was discussed and built. The restraint for this system that balanced multiple competing variables was primarily an active volume of 0.64 cm^3, a workspace clearance of at least an inch on every side, a field of 0.3T, and a local axial gradient of 13 T/m. The 3D electromagnetic finite element analysis modeling performed matched closely with experimental results. A series of magnetic seeds, were successfully characterized using a vibrating sample magnetometer. Finally, the magnetic seed was investigated under various flow conditions *in vitro* to analyze the effectiveness of the drug delivery system. The effectiveness of the drug delivery system was demonstrated under limiting assumptions of a specific magnetic field and gradient, seed material, a low fluid flow, and a small volume. The conclusions of this thesis are that magnetic targeted drug delivery is a viable technology and is still in its infancy and there is still much work to be completed before a clinical solution will fully emerge.

Chapter 6: Future Work

The future work in this field will involve a mutli-disciplinary approach from biologists, doctors, engineers, chemists, and other researchers. Although highly precise guidance was not demonstrated for magnetite microspheres, calculations in Chapter 3 predict accurate guidance will be attained and visibly demonstrated during a scheduled experiment using a modified optical system presently on order (Figure 45), 10 μm inner diameter tubing, and a fluid flow of 0.0005 m/s used in conjunction with the current system. The large magnetic workspace also allows us to in the future visually monitor the microspheres using a microscope equipped with long working distance objectives.

Figure 45. Zoom 160 Optical System modified with non-ferric components capable of micrometer resolution within the magnetic workspace.

Platform grouping of microspheres similar to the geometry of a nested "Russian doll" (Figure 46), where each doll contains an ever-decreasing smaller doll, are in need in order to address the controlling factors in targeting different sites. The grouping depends on the application's limiting parameters involved with counteracting fluid flow, tissue porosity, cell damage, and target resolution --from a large tissue area to a single cell and smaller. This method would involve encapsulating one-micron spheres inside of a 600-micron sphere that has a biodegradable coating that slowly dissolves *in vivo*. These

coatings generally take from hours to days to dissolve and release the smaller inner spheres. It has also been suggested that using multiple hydrogen bonding will give a similar fast unraveling capability that DNA does at 105°F. RF induction heating is one method that could give localized heating to break up the larger volume of magnetic microspheres into smaller more maneuverable spheres. This heating will take place when the carriers attempt to maneuver into smaller passageways and need the advantages that a smaller transport offers. These factors on the chemistry side of the magnetic drug delivery system need to be realized in order to maximize the targeting resolution of the magnetic stereotactic system.

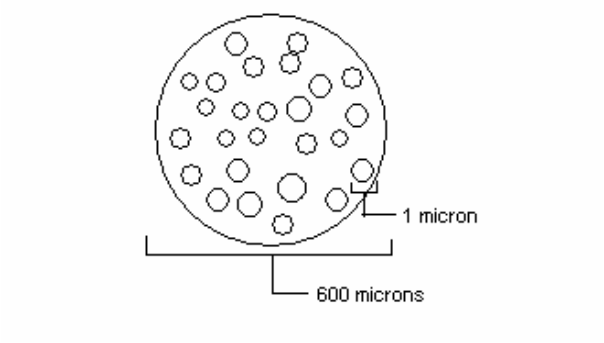

Figure 46. Platform grouping of microspheres.

A more compact and efficient design then the 5th generation MSS, 6-coil superconducting system could be implemented using MRI technology. The RF coils would take much less room then the fluoroscope hardware and would allow for larger fields/gradients since not all of the coils would have to be open bore to allow for imaging. The current procedure that Stereotaxis uses is to place the patient in a commercial MRI to get a roadmap of the pathway of interest and to update the position of the magnetic seed on that roadmap with data derived from the fluoroscope. The incorporation of MRI into the stereotaxis device will shorten and simplify the procedure that Stereotaxis, Inc. has followed in its current use of the TELSTAR to guide magnet tip catheters through the brain. The implementation of MRI with the fifth generation MSS is realizable since the practicality of low field MRI has been demonstrated for fields as low as the Earth's magnetic Field (5

x 10^{-7}T).[124] The 6-coil superconducting system offers advantages over other systems in that 4 of the coils may be operated as a quadruple magnet offering a higher gradient then the 12 T/m gradient calculated in the literature. Quadruple magnet configurations offer some of the highest gradients found to date.

The use of pulse magnets in combination with the above system may also be used when the target site limits the volume of the magnetic sphere. Pulse magnets would give a very high field and gradient and effectively will give a final hard push of the seed into the target location.

Other options less mature for targeted drug delivery are the further development of Micro Electronic Mechanical Systems (MEMS). MEMS devices have decreased the size of motors to the equivalence in size of smaller parasite and bacteria, enabling them to manipulate the body in similar ways that these creatures already possess. In order to conserve space and make these seeds smaller, one can have the power source be external to the machine. Having an external power source and coupling the energy into the system in much the same way that a crystal radio works allows the machine to have significant power available to it while keeping the overall size of the machine small. In effect, locally powered smart dust consisting of MEMS motors and actuators moving through the body in a remote controlled mini submarine.

The contributions to science given by this thesis are a literature review of prior and current magnetic guidance systems, electromagnetic analysis of the force anticipated on magnetic microspheres due to external magnetic fields and gradients, initial experimental results using electromagnets and fixed magnet systems to demonstrate magnetic microsphere clustering and controlled motion. It is the hope that careful review of this paper would further the necessary information background to bring the science fiction of manipulating the micrometer and nanometer scale with the same ease in which we manipulate the centimeter and millimeter scale with our fingers.

---

[124]C.L. Partain, R.R. Price, J.A. Patton, M.V. Kulkarni, A.E. James. *Magnetic Resonance Imaging,* ed., Saunders, Philadelphia, 1988.

Appendix A: Magnetic Variables in CGI and SI Units[125]

Quantity	Symbol	Gaussian & CGS emu[a]	Conversion Factor, C[b]	SI & Rationalized mks[c]
Magnetic flux density, Magnetic induction	B	gauss (G)[d]	10^{-4}	tesla (T), Wb/m^2
Magnetic Flux	ϕ	maxwell (Mx), $G \cdot cm^2$	10-8	weber (Wb), volt second (V·s)
Magnetic potential difference, magnetomotive force	U, F	gilbert (Gb)	$10/4\pi$	ampere (A)
Magnetic field strength, magnetizing force	H	oersted (Oe),[e] Gb/cm	$10^3/4\pi$	A/m[f]
(Volume) magnetization[g]	M	emu/cm^3[h]	10^3	A/m
(Volume) magnetization	$4\pi M$	G	$10^3/4\pi$	A/m
Magnetic polarization, intensity of magnetization	J, I	emu/cm^3	$4\pi \times 10^{-4}$	T, Wb/m^2[i]
(Mass) magnetization	σ, M	emu/g	1 $4\pi \times 10^{-7}$	$A \cdot m^2/kg$ $Wb \cdot m/kg$
Magnetic moment	m	emu, erg/G	10^{-3}	$A \cdot m^2$, joule per tesla (J/T)
Magnetic dipole moment	j	emu, erg/G	$4\pi \times 10^{-10}$	$Wb \cdot m$[i]
(Volume) susceptibility	χ, κ	dimensionless emu/cm^3	- $(4\pi)^2 \times 10^{-7}$	Henry per meter (H/m), Wb/(A·m)
(Mass) susceptibility	χ_ρ, κ_ρ	cm^3/g, emu/g	$4\pi \times 10^{-3}$ $(4\pi)2 \times 10^{-10}$	m^3/kg $H \cdot m^2/kg$
(Molar) susceptibility	χ_{mol}, κ_{mol}	cm^3/mol, emu/mol	$4\pi \times 10^{-6}$ $(4\pi)^2 \times 10^{-13}$	m^3/mol $H \cdot m^2/mol$
Permeability	μ	dimensionless	$4\pi \times 10^{-7}$	H/m, Wb/(A·m)
Relative permeability[j]	μ_r	not defined	-	dimensionless
(Volume) energy density, energy product[k]	W	erg/cm^3	10^{-1}	J/m^3
Demagnetization factor	D, N	dimensionless	$1/4\pi$	dimensionless

NOTES:

a. Gaussian units and cgs emu are the same for magnetic properties. The defining relation is $B = H + 4\pi M$.

b. Multiply a number in Gaussian units by C to convert it to SI (e.g. 1 G x 10^{-4}T/G = 10^{-4}T).

c. SI (Système International d'Unités) has been adopted by the National Bureau of Standards. Where two conversion factors are given, the upper one is recognized under, or consistent with, SI and is based on the definition $B = \mu_0(H + M)$, where to $\mu_0 = 4\pi \times 10^{-7}$H/m. The lower one is not recognized under SI and is based on the definition $B = \mu_0 H + J$, where the symbol I is often used in place of J.

d. 1 gauss = 10^5 gamma (γ).

e. Both oersted and gauss are expressed as $cm^{-½} \cdot g^{½} \cdot s^{-1}$ in terms of base units.

f. A/m was often expressed as "ampere-turn per meter" when used for magnetic field strength.

g. Magnetic moment per unit volume.

h. The designation "emu" is not a unit.

i. Recognized uder SI, even thoug based on the definition $B = \mu_0 H + J$. See footnote c.

j. $\mu_r = \mu/\mu_0 = 1 + \chi$, all in SI. μ_r is equal to Gaussian μ.

k. $B \cdot H$ and $\mu_0 M \cdot H$ have SI units J/m^3, $M \cdot H$ and $B \cdot H/4\pi$ have Gaussian units erg/cm^3.

R.B. Goldfarb and F.R. Fickett, U.S. Department of Commerce, National Bureau of Standards, Bolder, Colorado 80303, March 1985, NBS Special Publication 696. For sale by the Superintendent of Documents, U.S. Government Printing Office, Washington, D.C. 20402.

[125] User's Manual. Lakeshore 7300 Series. VSM System. February 2001.

Vita

Jeffrey Leach was born in Midlothian, VA on July 20, 1979. After finishing high school in Midlothian, VA he went to Virginia Tech in Blacksburg, VA to study electrical engineering. He completed a one-year co-op with Virginia Power at the North Anna Nuclear Power Plant during his undergraduate curriculum. Immediately after receiving his undergraduate degree in Electrical Engineering, he started work as a Graduate Research Assistant with Dr. Richard O. Claus at the Fiber and Electro-Optics Research Center. He also has become an avid caver (NSS-50977), amateur radio operator (KG4SUB), scuba diver, skydiver (A-41629), and pilot (FF0524272).

Jeffrey Harold Leach